uOttawa

L'Université canadienne
Canada's university

FACULTÉ DES ÉTUDES SUPÉRIEURES ET POSTOCTORALES

uOttawa

L'Université canadienne
Canada's university

FACULTY OF GRADUATE AND POSDOCTORAL STUDIES

M. A. Al-Mamun Bhuiyan
AUTEUR DE LA THÈSE / AUTHOR OF THESIS

M.A.Sc. (Biomedical Engineering)
GRADE / DEGREE

Department of Chemical and Biomedical Engineering
FACULTÉ, ÉCOLE, DÉPARTEMENT / FACULTY, SCHOOL, DEPARTMENT

Modeling and Development of a Magnetic Shielding Mechanism

TITRE DE LA THÈSE / TITLE OF THESIS

Tofy Mussivand
DIRECTEUR (DIRECTRICE) DE LA THÈSE / THESIS SUPERVISOR

CO-DIRECTEUR (CO-DIRECTRICE) DE LA THÈSE / THESIS CO-SUPERVISOR

Michel Labrosse

Donald Russell

Gary W. Slater
Le Doyen de la Faculté des études supérieures et postdoctorales / Dean of the Faculty of Graduate and Postdoctoral Studies

Modeling and Development of a Magnetic Shielding Mechanism

M. A. Al-Mamun Bhuiyan

Thesis submitted to the

Faculty of Graduate and Postdoctoral Studies

In partial fulfillment of the requirements for the degree of

Master of Applied Science in Biomedical Engineering

Ottawa-Carleton Institute for Biomedical Engineering and

Medical Devices Innovation Institute

University of Ottawa

Your file Votre référence
ISBN: 978-0-494-74179-5
Our file Notre référence
ISBN: 978-0-494-74179-5

Abstract

Background: Medical devices relying on biosignal acquisition are susceptible to electromagnetic interference. Current approaches are ineffective at shielding low amplitude, low frequency biosignal measurements. **Objective:** To develop a magnetic shielding mechanism to improve shielding effectiveness (SE) for low amplitude application. **Method:** A three layer shielding mechanism with the two inner layers made of cold rolled (CR) steel and an outer layer of aluminum (Al) was investigated. Modeling and simulations were performed using finite element analysis. Experiments were performed on shielding samples of CR steel and Al. **Results:** (1) The average SE for the three layer system was found to be 56.02 and 47.38 decibel by simulation and experiment respectively. (2) By incorporating a conductive layer of Al, performance was investigated up to 25 KHz. SE was observed to increase with the increase in interfering signal frequency. **Conclusion:** The proposed shielding mechanism would reduce the interference level of low amplitude, low frequency biosignal measurements.

Acknowledgements

I would like to dedicate this thesis to my father, who spent all of his savings and pension just to make one dream come true. I would also like to thank my mother and other family members for their endless support and encouragement. Without them, I am nothing.

I am grateful and indebted to my supervisor Dr. Tofy Mussivand, Medical Devices Innovation Institute, University of Ottawa, for his excellent support, advices, and expertise. He always guided me in the right direction. Without his contribution, this work would not have been possible.

I am also indebted to my co-workers Bashir Morshed and John Szalas at Medical Devices Innovation Institute for inspiring me throughout and most importantly for helping me revise this thesis.

A very special thanks to my wife Melita, to be right beside me during those frustrating summer nights and annoying me always by saying: "If you think you can, you can."

Continuous effort - not strength or intelligence - is the key to unlocking our potential.

- Liane Cordes

Table of Contents

List of Figures

List of Tables

List of Symbols

B	Magnetic flux density
H	Magnetic field strength
D	Electric displacement field
$\nabla.$	Divergence operator
∇x	Curl operator
ε	Electrical permittivity of a medium
μ	Magnetic permeability of a medium
σ	Electrical conductivity of a medium
α	Attenuation constant
γ	Propagation constant
δ	Skin depth parameter
Δ	Material Thickness
t	Time
f	Frequency
E	Electric field strength
J	Free current density
Z	Characteristic impedance

k	Wave number in a medium
R	Reflection loss term
A	Absorption loss term
G	Magnetic Potential
M	Multiple reflection term
m	Magnetic moment
I	Current in amps
r	Radius of current loop
λ	Arbitrary chosen constant

List of Acronyms

3D	Three Dimensional
AC	Alternating Current
Al	Aluminum
AWG	American Wire Gauge
CR Steel	Cold Rolled Steel
CSD	Cortical Spreading Depression
DC	Direct Current
dB	Decibel
EEG	Electroencephalography
EMF	Electro Magnetic Field
EMI	Electro Magnetic Interference
FEM	Finite Element Method
MEG	Magnetoencephalography
SE	Shielding Effectiveness

Chapter 1: Introduction

1.1 Background and Motivations

Mental and neurological disorders are among the most prevalent and complicated diseases. Among all the neurological disorders, migraines, epilepsy, sleep related disorders are the key problems where healthy lives are being lost to disability each year [1]. A study conducted by the World Health Organization reports that mental and neurological disorders together are responsible for 30.8% of disability worldwide and migraines alone are 1.4% making it to be within the top 20 causes of disability [2]. Proper diagnosis of these disorders is still a challenge due to the electromagnetic interference (EMI) problem associated with the current instrumentation [3].

Magnetoencephalography (MEG), electroencephalography (EEG) are used for diagnosing neurological disorders by sensing very low amplitude brain signals [4;5]. MEG is a technique that monitors brain activity by sensing the weak magnetic field produced by the electrical activity of the brain. An array of sensors known as the SQUID (superconducting quantum interference device) is used to detect the brain signals. On the other hand, EEG is the technique of monitoring brain activity by sensing electrical signals of the brain. Researchers suggest that measurement of low amplitude brain signals can potentially help

with accurate diagnosis of many neurological disorders. For example, cortical spreading depression (CSD) can play an important role in the diagnosis of migraine [6]. CSD is defined as the transient cellular depolarization that propagates over the cortex. The detection of CSD involves the measurement of low frequency, low amplitude brain signals. MEG and EEG are also often used in combination with functional magnetic resonance imaging for better spatial and temporal resolution at the same time [7-9]. However, medical devices such as MEG and EEG are highly disturbed by the external magnetic noise sources and need to be protected. Hence, such diagnostic measurements need to be performed in presence of suitable magnetic shielding [3;4;10;11].

1.1.1 Current Methods and Techniques of Magnetic Shielding

Magnetic shielding is the countermeasure to reduce the effect of EMI in an area of interest. Different types of magnetic shielding techniques to assist in brain and other biomagnetic signal measurement have been proposed. The shielding structures proposed by various researchers include, but are not limited to, spherical shapes, long pipes, sealed cubes, and cylinders [12-14]. Brain and other biomagnetic measurements are typically done in a magnetically shielded room. Such rooms are made of ferromagnetic materials such as mu-metals [15;16] or Permalloy [17]. For a magnetically shielded room the shield size and material weight are large, and therefore associated costs are high [18]. Therefore, magnetic shielding is often designed to encompass limited space. High performance cylindrical magnetic shields made of Permalloy, Finemet, and cobalt based ribbons were demonstrated by some researchers [19-21]. Zhao *et al.* investigated the shielding performance of rectangular metal shielding with an aperture covered with wire grid [22]. Recently, Takeshi Saito proposed open type magnetic shielding structures using elongated strips of Permalloy

and grain oriented electromagnetic steel sheets [12;23]. Fujikura *et al.* also investigated the properties of a cube shaped magnetic shielding structure using four open type magnetic shield walls [24]. Hirano *et al.* proposed and investigated the performance of a two layered open type magnetic shielding in a nested arrangement using the strips of grain oriented electromagnetic steel sheets [25]. While these open type magnetic shielding structures solve the issue of the user's inconvenience due to the conventional closed structure, the shielding performance of a closed structure is comparatively high [25].

1.1.2 Current Issues

One common limitation related to most conventional shielding systems is that shielding effectiveness decreases at low frequency whereas the magnetic noise increases [6]. The common sources of external magnetic noise are electrical facilities, power lines, switching circuits, the earth's magnetic fields or the environmental noise produced by cars, and trains [22;26-30]. Such magnetic noise sources interfere with the brain signals detected by MEG and EEG and make the measurement of low amplitude brain signals problematic. As a result, it is important to develop a mechanism that can improve the effectiveness of a shielding system and potentially help with diagnosis of neurological disorders.

Another limitation of magnetic shielding can be its failure to effectively protect a device from quasi static interference sources. A magnetic noise source with extremely low frequency is called quasi-static source. At extremely low frequency the magnetic noise source works as a static field source. But due to its slowly alternating nature it is not entirely static and termed as a quasi-static source. To shield an area from such a low frequency magnetic noise source, two different types of shielding mechanisms, static shielding and dynamic shielding, must be considered [31]. A static shielding mechanism is independent of

the noise source frequency. For such a mechanism, shielding efficiency depends on the material's relative permeability. Shielding efficiency increases with the relative permeability of the shielding material. On the other hand, a dynamic shielding mechanism is dependent on the frequency of the magnetic noise source. For such a mechanism, shielding efficiency depends on the material's electrical conductivity. Shielding efficiency increases with the frequency of the magnetic noise source and the electrical conductivity of the shielding material. However, there are no known materials that have the properties of both high permeability and high electrical conductivity at the same time. One solution to this problem could be to make the shielding system multilayered, with materials in different layers [14;16;31;32].

The thesis aims to investigate different parameters of magnetic shielding and based on simulation, and experimental results suggesting a shielding mechanism that can improve the performance of a magnetic shielding. Magnetic shielding with improved effectiveness can reduce the interference level of MEG and EEG from outside noise sources. This can increase the detected brain signal to noise ratio and potentially help in the diagnosis of mental and neurological disorders.

1.2 Objectives

The goal of this thesis is to develop a magnetic shielding mechanism with improved shielding effectiveness (SE). This can potentially be achieved by increasing the number of shielding surfaces in a multilayered system which could increase the surface reflection loss. Incorporation of different shielding materials in different layers will also be investigated. In order to obtain the overall goal of developing a magnetic shielding mechanism that can potentially be used to improve the SE, a number of steps were defined. They are:

1. Investigate different aspects of magnetic shielding and identify parameters, conditions and/or ideas that might improve the effectiveness of a shielding system.
2. Utilize different types of material in different layers to ensure the reliability of the shielding system for different frequency ranges.
3. Conduct simulation studies to evaluate the validity and performance of the proposed shielding mechanism.
4. Conduct laboratory experiments to demonstrate the idea under real world conditions.
5. Compare and discuss the simulation results and the results found experimentally.

1.3 Key Results

It was found both by running simulations and experiments that effectiveness of a magnetic shielding system could be improved by increasing the number of shielding surfaces. Shielding surface was increased by introducing new layers. Cold rolled steel (CR steel) and Aluminum (Al) were used to investigate the performance of the magnetic shielding. Initially, for a two-layer system with CR steel as the shielding material, the effectiveness could be improved by 11.2% compared to a single layer system of equivalent thickness as confirmed by both simulation and experimental results. The incorporation of Al in a separate external layer that made it a three-layer system improved the performance of the shielding system at low frequencies and the effectiveness tends to increase with the frequency of the interfering magnetic noise source. Finally, a three layered magnetic shielding was proposed. The proposed three-layer magnetic shielding, with one outer layer of Al and two inner layers of CR steel, gave a shielding effectiveness of 56.02 and 47.38 decibels for simulation and experimental results respectively.

1.4 Thesis Contribution

The following is a list of the main research contributions demonstrated in this thesis which will be explained thoroughly in the chapters to follow:

1. Introduced a magnetic shielding mechanism comprised of three layers: two layers with magnetic material and one layer with conductive material. CR steel was used as the magnetic material that formed the inner two layers and Al was used as the conductive material to form the outer layer.
2. The magnetic shielding mechanism was demonstrated to improve the shielding effectiveness and the introduction of conductive material Al improved the performance of shielding system further, especially at higher frequencies.

1.5 Thesis Outline

Chapter 1 covers the overview and motivations behind this work. Key results and thesis contributions are also presented.

Chapter 2 provides background information on electromagnetic waves, electromagnetic interference problems, different types of interfering sources, and current techniques for shielding against electromagnetic interference, their relative importance and limitations, different types of shielding materials and their applications towards designing a shielding system.

Chapter 3 covers the mathematical modeling of different types of electromagnetic sources and a planar magnetic shielding in presence of circular current loop. It also discusses the effect of different parameters on shielding performance by referring to the mathematical equations.

Chapter 4 introduces the systematic work flow diagram for use in the development of a shielding mechanism. It describes the simulation environment, finite element analysis method, boundary conditions, parametric model creation, and simulation results with supporting graphs and data.

Chapter 5 discusses the experimental methods, equipment, preparation of the shielding samples and experimental data with supporting graphs and figures.

Chapter 6 compares the simulation results with experimental findings and discusses possible discrepancies and general trends.

Chapter 7 concludes the thesis by giving a summary of the major findings and a list of recommendations for future work.

Chapter 2: Literature Review

This chapter introduces background information on electromagnetic waves, electromagnetic interference problems, different types of interfering sources, current techniques of shielding against electromagnetic interferences, and their relative importance and limitations.

2.1 Electromagnetic Field

An electromagnetic field (EMF) is produced by electrically charged objects or their movements. EMF can be thought of as the combination of an electric field and a magnetic field. Both electric (E-field) and magnetic fields (H-field) are oscillating at right angles to each other [33]. An E-field is generated by stationary charges. A circuit with high impedance that creates a potential difference gives rise to an E-field. On the other hand, an H-field is generated by moving charges. A circuit with low impedance where current is flowing gives rise to an H-field [31]. The unit for E-field and H-field are respectively volt/meter and ampere/meter.

Figure 2-1 shows a plane polarized electromagnetic field travelling along the Z-axis direction. Here the E-field is oscillating along the X-axis and H-field is oscillating along the Y-axis. The angular frequency of this wave is given by 'ω', where $\omega = 2\pi f$, f being the frequency of the wave.

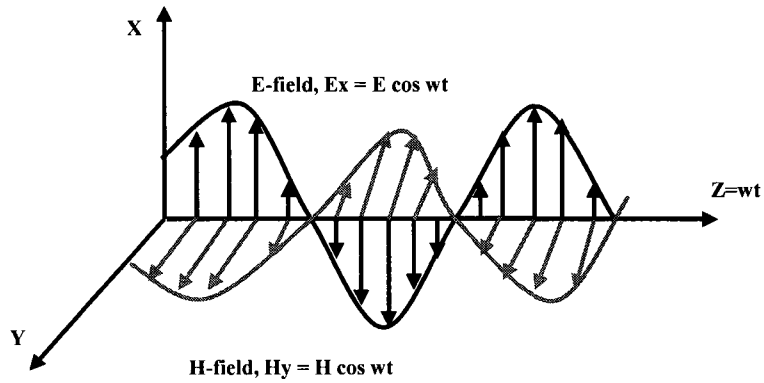

Figure 2-1: An electromagnetic waveform. E-field and H-field are oscillating in different planes (adapted from [33]).

2.2 Maxwell's Equations of Electromagnetics

Maxwell's equations are the governing equations for electromagnetics. Maxwell's equations are a set of four partial differential equations (they can also be expressed in integral form) that define the behaviour of electromagnetic waves. The partial differential equations are known individually as the Gauss' law, Gauss' law for magnetism, Faraday's law and Ampere's circuital law. The laws are given below [34]:

$$\nabla . \vec{D} = \frac{\rho}{\varepsilon_0} \tag{2.1}$$

$$\nabla . \vec{B} = 0 \tag{2.2}$$

$$\nabla x \vec{E} = -\frac{\partial \vec{B}}{\partial t} \tag{2.3}$$

$$\nabla x\vec{H} = \vec{J} + \frac{\partial \vec{D}}{\partial t} \qquad (2.4)$$

Where, '*B*' is the magnetic flux density, '*H*' is the magnetic field strength, '*D*' is the electric displacement field, '∇.' is the divergence operator, '∇x' is the curl operator, 'ρ' is the charge density, '*t*' is the time and ε_0 is the permittivity of free space. Equations (2.1) through (2.4) explain electromagnetic field behaviour and are the fundamental relations that describe the magnetic shielding mechanism.

2.3 Electromagnetic Interference

With the advent of technologies that use the electromagnetic spectrum such as wireless telephone, electronic surveillance systems, high voltage power lines, transformers, welders, magnetic resonance image scanners, electro surgical tools, defibrillators, and neurostimulators, electromagnetic interference (EMI) with medical devices has increased [35]. An electromagnetic wave can interfere with the activity of other medical devices in two ways: conduction and radiation. Conducted electromagnetic interference occurs due to a direct connection of electrical cables or wires between emitter system (EMI source) and the susceptor system (the system that gets interfered with). This thesis work deals with the second type of EMI, i.e. radiated EMI. Radiated EMI does not require a direct connection of electrical cables or wire between emitter and susceptor system. From now onwards, the discussion will be confined to the realm of radiated EMI, their sources and countermeasures. Figure 2-2 shows the two types of EMI and manner in which they interfere with the susceptor system.

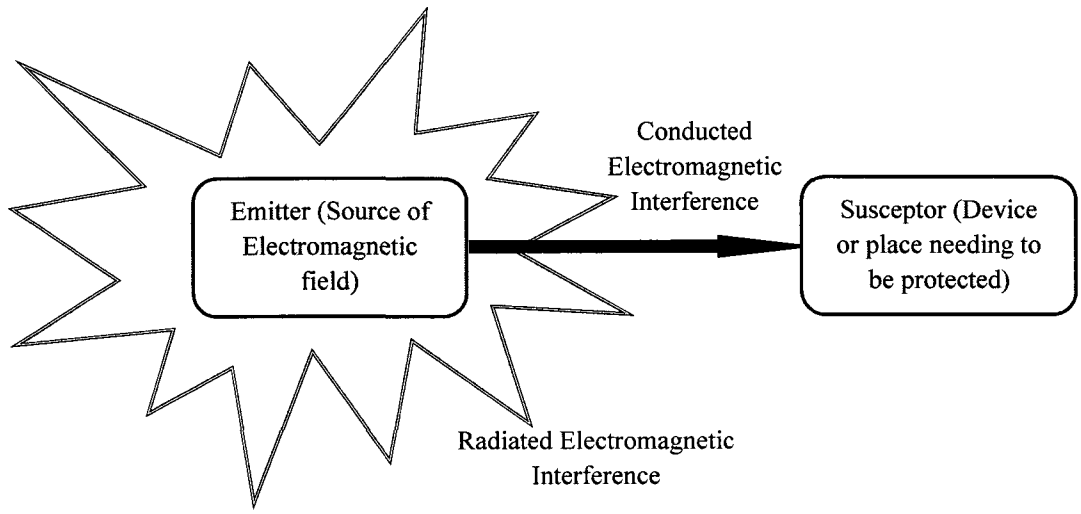

Figure 2-2: Electromagnetic wave generated from an emitter system is interfering with a susceptor system through conduction and radiation

2.4 Interference Sources and Types

Different types of EMI sources play significant roles in modeling and designing aspects of a shielding system. The behaviour of a particular shielding design is partially dependent on source type. Hence an understanding of the characteristics of different EMI source is necessary. EMI sources can be classified based on their types and frequencies of energy emission. Depending on their frequency, they can be divided into three broad categories: static EMI sources, dynamic EMI sources, and quasi-static EMI sources.

2.4.1 Static Field Sources

The other name for static field sources is DC (direct current) magnetic field sources [36]. The emitted magnetic field from this type of sources does not vary with time [31]. This means their frequency of oscillation is zero. They can be created by a steady flow of electric charges or by a permanent magnet and can interfere with the operation of some medical

devices. The most common source of static magnetic field is the earth's natural magnetic field and permanent magnets used in different electric and medical imaging technologies. The strength of earth's magnetic field is typically 50 μT and varies from 30 to 70 μT depending on the geographic locations. The other sources of static magnetic fields are magnetic imaging technologies, electric trains, and electric appliances using DC current. All these sources can interfere with medical devices and need to be shielded for accurate operation of those devices.

2.4.2 Dynamic Field Sources

The magnetic field strength emitted from a dynamic field source varies with time. They are frequency dependent sources [31]. For example, when an AC (alternating current) passes through a conductor, dynamic magnetic field is created. Depending on the oscillations, dynamic sources can be further subdivided into low frequency, intermediate frequency and high frequency sources. Wall power supply based electronic devices emit low frequency EMI. Computer screens, anti theft devices fall under the intermediate frequency sources. Lastly, microwave (MW) oven, radar, cell phones, and TV are high frequency sources. All of these are potential sources of EMI and can interfere with the operation of medical devices [26;37].

2.4.3 Quasi-Static Field Sources

The term 'quasi' means 'like something' or 'resembling'. As the name implies, 'quasi-static' means sources that act like static sources. Quasi-static field sources are very low frequency sources. As they are of very low frequency, they act like a static field source. But as their source is very slowly changing they are not entirely static and called quasi-static field. For

example, EMI generated from 50 or 60 Hz power lines are quasi-static in nature. As these types of sources have the properties of both static and dynamic sources, shielding against such sources need attention in both fields [31].

2.5 Magnetic Shielding Mechanism

A countermeasure to reduce the effect of electromagnetic interference is very important especially for medical devices. Shielding is an effective way to mitigate the effect of electromagnetic interference in an area of interest. The place is then considered to be 'shielded'. The idea of the magnetic shielding is to redirect magnetic fluxes by any means so that they do not enter the area of interest. By altering the spatial distribution of the electromagnetic field, shielding mitigates or reduces the effects of electromagnetic interference. Any shielding mechanism aims to prevent a particular device to radiate electromagnetic fields outside its barrier or prevent external magnetic source to interfere with the inside device. Typically, a shielding system utilizes one of the following ideas:

1. Placing a screen between the emitter system and the susceptor system and protecting the susceptor system from the effect of radiated electromagnetic wave [25].
2. Diverting the electromagnetic field to a path of low reluctance (reluctance in magnetism is analogous to resistance in electrical circuit theory) by introducing a suitable medium. This technique is known as the 'flux diversion technique' or sometimes as 'flux shunting'.
3. Placing a screen between the emitter and the susceptor system with high electrical conductivity [38;39]. In presence of the interfering electromagnetic field, the screen

generates its own field in opposite direction to minimize the interfering effect. This is known as the 'eddy current cancellation' technique.

4. Combination of two or more of the above ideas.

Mathematically, shielding is the way of introducing attenuation loss to the electromagnetic wave when it is impinging on a medium. The amount of loss depends on the characteristics of the medium used as the shielding screen. If the propagation constant of an impinging electromagnetic wave in a medium is defined by 'γ' it can be shown that,

$$\gamma = \sqrt{j\omega\mu(j\omega\varepsilon + \sigma)} = \alpha + j\beta \qquad (2.5)$$

Where, μ, ε and σ are respectively the permeability, permittivity and conductivity of the medium. In the above equation (2.5), 'α' is the attenuation constant and accounted for the loss in the medium. This means loss depends on the permeability and electrical conductivity of the shielding material.

2.5.1 Shielding effectiveness

The main goal of a shielding system is to improve the shielding effectiveness (SE) of the location of interest. SE is the measure of electromagnetic field level reduction at a point by placing the shielding system in between the emitter and the susceptor system. In other words, it is the measure of attenuation of an electromagnetic field at a certain point by placing the shielding system in between emitter and susceptor. SE is measured in decibels (dB). To measure the SE of a system placed between the interfering magnetic source and the

point where measurement is being made, two measurements of the electromagnetic field strength must be taken at that point. One measurement would be in presence of the shielding screen and other in absence of the screen. The ratio of the two values of the field strength before and after placing the shield when transferred to decibel indicates the SE [22;25;40;41]. Mathematically it can be shown as,

$$SE = 20\log_{10}\left(\frac{H_{p,without}}{H_{p,with}}\right) \quad (2.6)$$

Where $H_{p,\ without}$ and $H_{p,\ with}$ is the magnetic field strength measured at point 'P' without and with placing the shield respectively. SE can be defined in terms of electric field E also as,

$$SE = 20\log_{10}\left(\frac{E_{p,without}}{E_{p,with}}\right) \quad (2.7)$$

Where $E_{p,\ without}$ and $E_{p,\ with}$ is the electric field strength measured at point 'P' without and with placing the shield respectively. These concepts are shown in Figure 2-3.

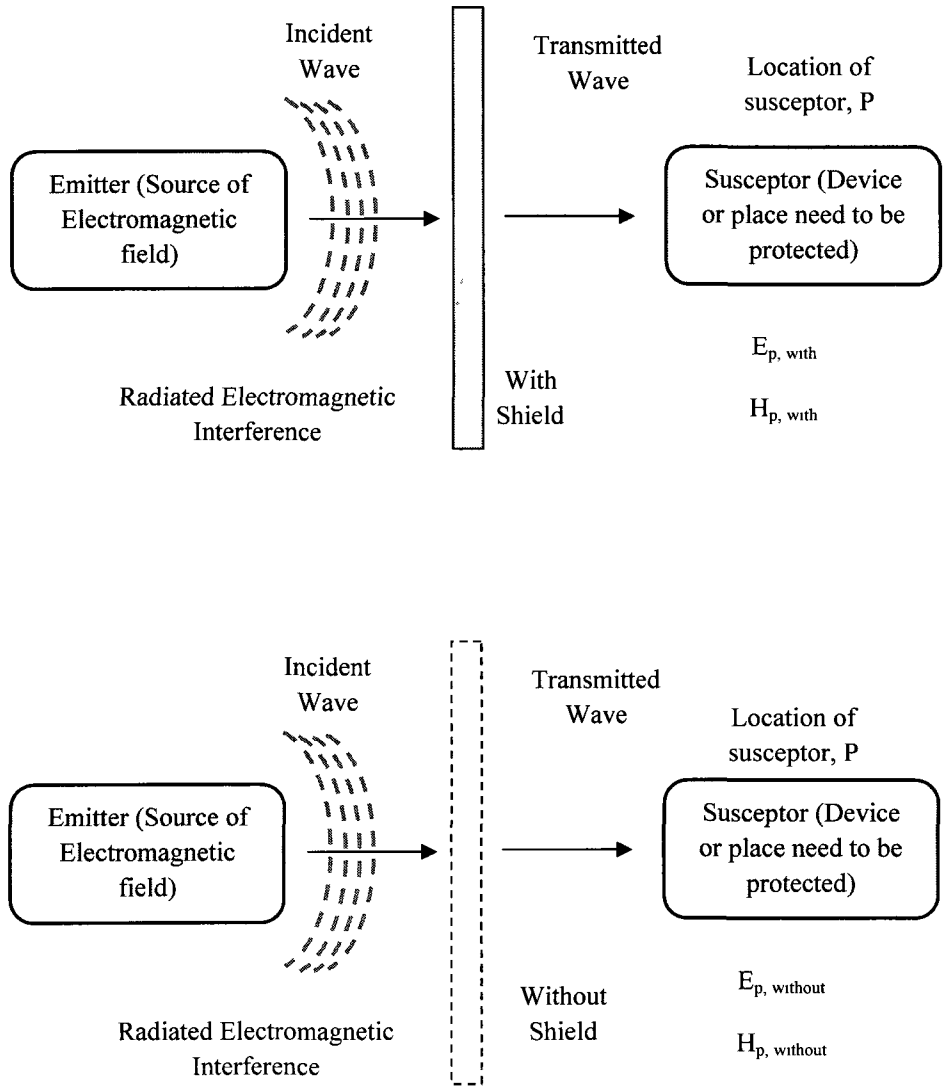

Figure 2-3: (Top) Measurement of E-field and H-field at point P (location of the susceptor system) with placing the magnetic shield in between. (Bottom) Measurement of E-field and H-field at point P (location of the susceptor system) without placing the magnetic shield in between

2.5.2 Magnetic Flux Diversion

Magnetic flux diversion technique is also widely known as the flux shunting mechanism. This technique of flux diversion is governed by Gauss's law and Ampere's circuital law. The differential form of Gauss's law for magnetism can be shown mathematically as,

$$\nabla . \vec{B} = 0 \qquad (2.8)$$

Where, '∇.' is the divergence operator and 'B' is the magnetic flux density.

And the differential form of Ampere's circuital law can be shown as,

$$\nabla \times \vec{H} = \vec{J} + \frac{\partial \vec{D}}{\partial t} \qquad (2.9)$$

Where '$\nabla\times$' is the curl operator, 'J' is the free current density, 't' is the time, and 'D' is the electric flux density.

A scenario where the magnetic flux from a source is impinging on a ferromagnetic material from air, Gauss's law of magnetism requires that the normal component of the magnetic flux density 'B' be continuous at the air-metal interface. On the other hand, Ampere's circuital law requires that the tangential component of the magnetic field intensity 'H' be continuous at the interface [42;43]. Both these conditions need to be simultaneously satisfied. Hence at the air and shielding material interface, the magnetic flux density is nearly perpendicular to the surface. On the other hand, at the shielding material side of the interface, the magnetic flux density is guided along the shield nearly tangential to the surface. As a result, magnetic field produced by a source is guided along the shielding material when impinging upon it and eventually partially transferred back to the initial medium [44]. This technique of magnetic shielding is known as the magnetic flux diversion technique. The amount of flux

diversion can be increased by either taking material with higher magnetic permeability or by increasing the material thickness or both. The mechanism is shown graphically in Figure 2-4.

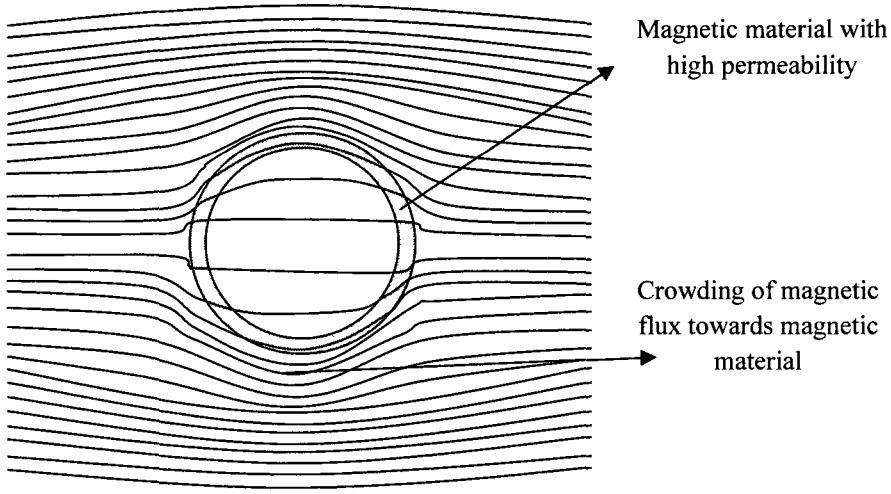

Figure 2-4: Magnetic flux diversion technique. Transmitted wave is attenuated on the other side of the magnetic material as impinging wave is diverted and crowded towards the high permeable magnetic material (adapted from [45]).

2.5.3 Eddy Current Cancellation

Eddy current cancellation technique is governed by Faraday's law of induction. Faraday's law of induction states that in a closed circuit the induced electromotive force is equal to the time rate of change of the magnetic flux. Faraday's law of induction is bilateral. That means an alternating electromotive force will also induce a changing magnetic flux. Faraday's law of induction can be shown mathematically as,

$$\nabla \times \vec{E} = -\frac{\partial \vec{B}}{\partial t} \qquad (2.10)$$

Where '$\nabla\times$' is the curl operator, 'E' is the electric field, 't' is the time, and 'B' is the magnetic flux density.

According to this law, if a conductive material is placed in a time varying magnetic field, an electromotive force will be induced. This induced electromotive force will generate a rotating current in the conductive material. Since Faraday's law works both way, this current will also generate a time varying magnetic field opposite in direction to the original one. This counteraction of magnetic field results in the net lowering of the magnetic field in the vicinity. High conductive material [38] such as aluminum and copper are well suited to adopt this shielding technique. The induced current is widely known as the eddy current (or sometimes Foucault current) [31]. Therefore, this technique of magnetic shielding is known as the eddy current cancellation technique. The mechanism is depicted in Figure 2-5.

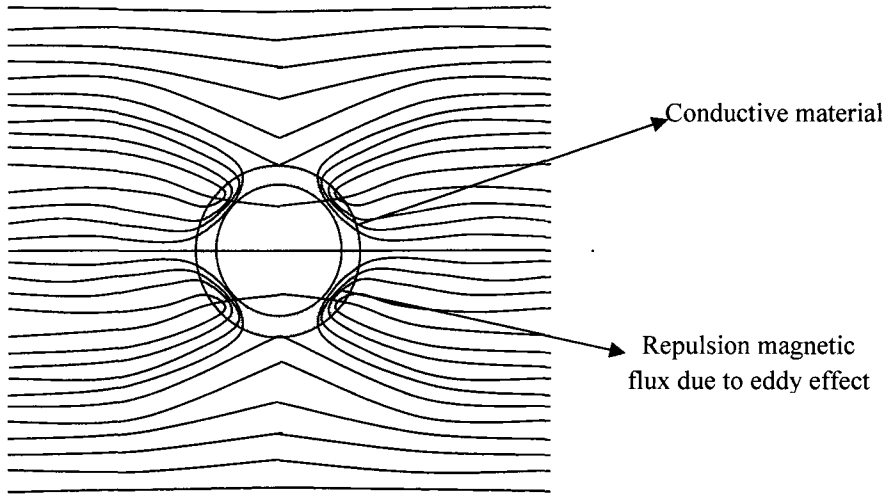

Figure 2-5: Eddy current cancellation technique. The incident wave is repulsed due to the generation of opposite directive localized magnetic field inside the conductive material (adapted from [45]).

2.5.4 Reflection and Absorption Phenomena

Reflection and absorption phenomena are two modes of weakening the signal strength of an impinging electromagnetic wave on a shield. In case of uniform planar waves, electric and magnetic field vectors remain in a single plane. For such waves, there are no amplitude and phase variation with time. Both fields remain in time phase. In other words, both electric and magnetic fields are coupled. Such a uniform planar wave suffers from reflection and absorption losses when incident on a shielding material.

Mathematically a plane wave can be defined as an electromagnetic wave in the frequency domain where electric field 'E' and magnetic field 'H' are given by,

$$\vec{E}\ (x,y,z) = \vec{E}_0 e^{-j(k_x x + k_y y + k_z z)} \tag{2.11}$$

$$\vec{H}\ (x,y,z) = \vec{H}_0 e^{-j(k_x x + k_y y + k_z z)} \tag{2.12}$$

Where 'E_0' and 'H_0' are constant vectors and k_x, k_y, k_z define the wave vector.

In Figure 2-6, the transverse direction of the plane wave is along the x axis. It is assumed that the medium at either side of the shielding material is air (Region 1 and 3). Region 2 represents inside of the shielding material. Let, the permeability and permittivity of air is μ_{air} and ε_{air} ; and that of shielding material is μ_s and ε_s . The wave number inside the shielding material is k_s and thickness of the shielding material is Δ.

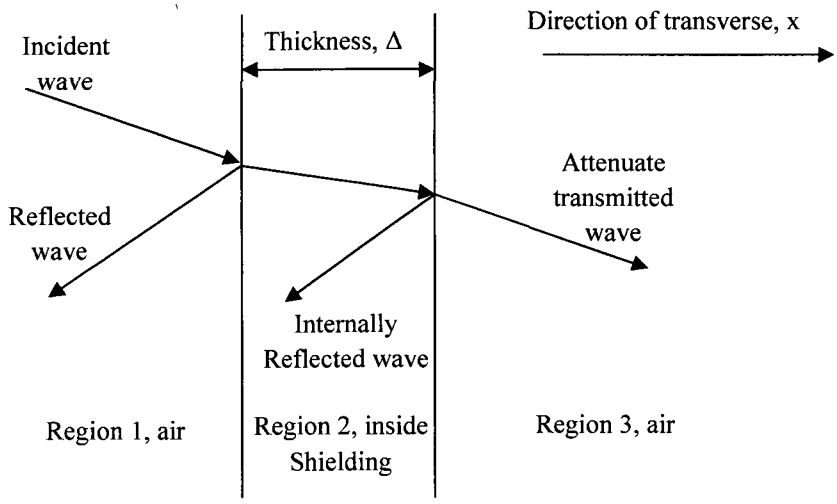

Figure 2-6: Reflection and absorption phenomena in a shielding material of thickness Δ. The wave is approaching along the x direction

As already described in equation (2.6), shielding effectiveness in region 3 can be written as,

$$SE = 20\log_{10}\frac{H_{3,without}}{H_{3,with}} \qquad (2.13)$$

Where $H_{3,\ without}$ and $H_{3,\ with}$ is the magnetic field in region 3 before and after placing the shield respectively. It can be mathematically shown that [45],

$$SE = -20\log_{10}\left(\frac{4Z_{air}Z_s}{(Z_{air}+Z_s)^2}e^{-jk_s\Delta}\frac{(Z_{air}+Z_s)^2}{(Z_{air}+Z_s)^2-(Z_{air}-Z_s)^2e^{-2jk_s\Delta}}\right) \qquad (2.14)$$

Or,

$$SE = R + A + M \qquad (2.15)$$

Where from the relationship it is evident that,

$$R = 20\log_{10}\left(\frac{(Z_{air}+Z_s)^2}{4Z_{air}Z_s}\right) \tag{2.16}$$

$$A = 20\log_{10}\left(e^{jk_s\Delta}\right) \tag{2.17}$$

$$M = 20\log_{10}\left(\frac{(Z_{air}+Z_s)^2-(Z_{air}-Z_s)^2e^{-2jk_s\Delta}}{(Z_{air}+Z_s)^2}\right) \tag{2.18}$$

Here, Z_{air} and Z_s indicate the characteristic impedance of the air and shielding material respectively. Where,

$$Z_{air} = \sqrt{\frac{\mu_{air}}{\varepsilon_{air}}} \tag{2.19}$$

$$Z_s = \sqrt{\frac{\mu_s}{\varepsilon_s}} \tag{2.20}$$

The term R in equation (2.15) and (2.16) represents the reflection loss term. When the wave is incident on the air-shield barrier, part of the incident wave is reflected back to its original medium and does not pass through. The amount of reflection loss depends on the mismatch between the two characteristic impedances Z_{air} and Z_s. As there is an impedance discontinuity in the air-metal interface, part of the incident wave is reflected back to air (initial medium). The amount of loss depends on the reflection coefficient of the two medium but not on the thickness of the shielding material. By increasing the number of shielding surfaces in a multilayered system SE can be improved. This increase in SE is predicted by Schelkunoff's transmission theory of shielding [46]. Such multilayered

shielding systems can be used to improve shielding effectiveness and has the potential for bio-magnetic measurements [16;47;48].

Term 'A' in equation (2.15) and (2.17) represents the absorption loss. This absorption loss term depends on the shielding material property. Absorption loss increases with the increase in material thickness, Δ and the relative permeability of the material.

The last term 'M' in equation (2.15) and (2.18) is known as the multiple reflection term. A plane wave when impinging on a shielding barrier, suffers multiple reflection as shown in Figure 2-6. Hence it is attenuated before transmitting through the shielding material. But this type of loss is negligible at higher frequencies and dominant at lower frequencies. At lower frequencies, 'M' can be of negative value. Figure 2-7 shows how reflection and absorption losses vary with the frequency in some common materials.

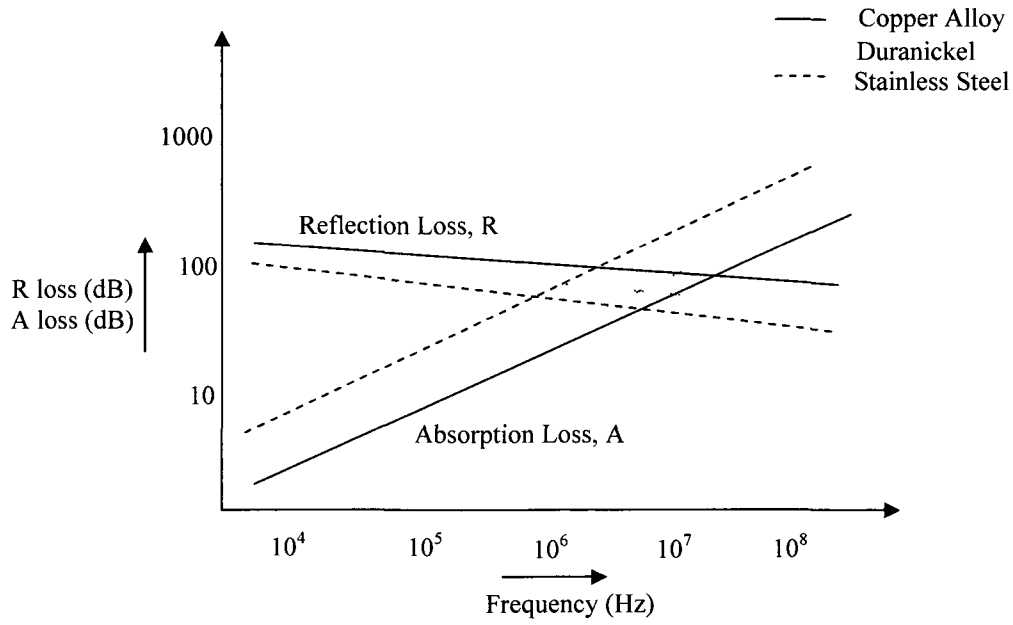

Figure 2-7: Variation of reflection loss term R and absorption loss term A with frequency in some common materials (adapted from [45]).

2.5.5 Magnetic Shaking

Magnetic shaking is an active process of shielding. Magnetic shaking is the process of superimposing a relatively strong alternating magnetic field on the disturbance magnetic field of the magnetic material [49]. This technique aims to reduce the effects of hysteresis losses. These types of losses are commonly seen in the magnetic materials. The effects of applying magnetic shaking current on a magnetic material are [50-52]:

1. Hysteresis curve narrows down and the slope of the magnetization curve increases.
2. Improves the incremental permeability of the magnetic materials.
3. It keeps the material's domain wall in vibrating motion.
4. Improves the shielding effectiveness of the material used.

One major problem related to the application of magnetic shaking is that it might increase the leakage flux in the area of interest. To avoid this problem, it is a common practice to use additional passive shielding layers inside to minimize the effect of magnetic flux leakage. The technique of superimposing an alternating magnetic field is shown in Figure 2-8.

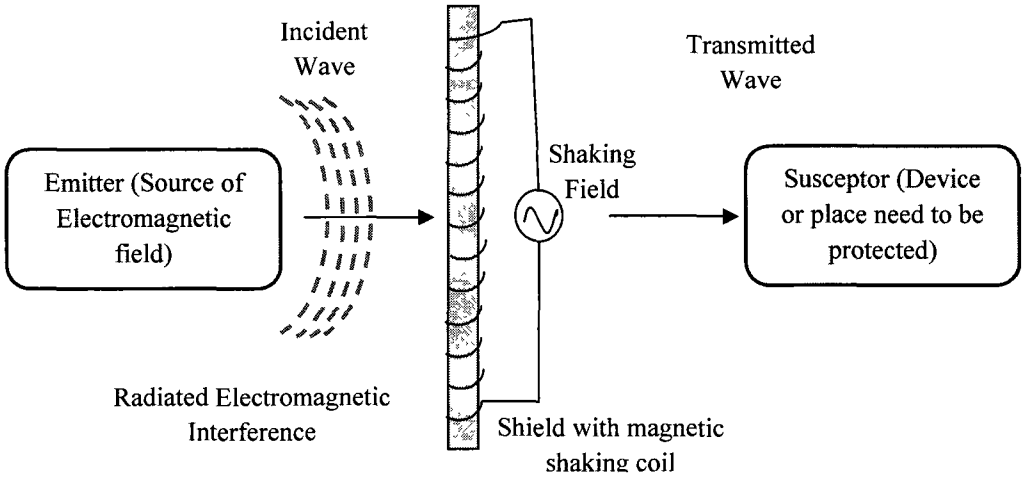

Figure 2-8: Illustration of magnetic shaking mechanism. Application of shaking field improves the incremental permeability and shielding effectiveness of the material

2.5.6 Static and Dynamic Shielding

Based on the frequency of the interfering magnetic source, there are two types of magnetic shielding mechanisms: static shielding and dynamic shielding. Static shielding mechanism is independent of the interfering source frequency. According to the governing equations of electromagnetics for a static field [53],

$$\nabla x\vec{H} = 0 \qquad (2.21)$$

$$\nabla.\vec{B} = 0 \qquad (2.22)$$

If μ is the magnetic permeability of the medium,

$$\vec{B} = \mu\vec{H} \qquad (2.23)$$

From the above relations, it can be deduced that,

$$\vec{H} = -grad\ \vec{G} \qquad (2.24)$$

Where, G is called the magnetic potential. From here it can be shown that,

$$\nabla.\left(\mu\, grad\, \vec{G}\right) = 0 \qquad (2.25)$$

For a constant value of μ the relation become,

$$\nabla^2 \vec{G} = 0 \qquad (2.26)$$

In order to determine the distribution of magnetic field the equation (2.26) needs to be solved. In addition, it should be mentioned here that shielding effectiveness of a static system depends on the thickness and magnetic permeability of the material used. Higher shielding effectiveness can be achieved with higher thickness and higher permeability. On the other hand, shielding effectiveness of a dynamic shielding system depends on the frequency of the interfering source. The effectiveness increases with the increasing frequency. The electrical conductivity of the material used also affects the shielding effectiveness. The higher the electrical conductivity, the higher the effectiveness. Static and dynamic shielding both depend on the thickness of the shielding material. In general, shielding effectiveness increases with increasing thickness of the shielding material.

In view of the fact that, quasi static sources have the properties of both static field and dynamic field; both shielding mechanisms are sometimes employed in a single system. The idea is to offer a multilayered shielding system. In such systems, materials are arranged in different layers where both static and dynamic shielding mechanism are utilized [14;16]. Highly magnetic permeable materials and conductive materials are placed in different layers to provide static and dynamic shielding respectively. This type of shielding systems is particularly suitable to protect a device from quasi static interfering sources.

2.6 Shielding Materials

Materials play a significant role in almost all types of magnetic shielding design. Material composition, magnetic properties, electrical conductivity, and physical dimensions are among the important design parameters of a magnetic shielding. Magnetic shielding is generally made of either conductive materials or ferromagnetic materials or combination of both. Considering the important role they play, a review of different shielding materials, their shielding mechanism, and how different parameters affect the performance of the shielding systems are discussed next.

2.6.1 Ferromagnetic Material

Magnetic materials are classified by magnetic susceptibility. Magnetic susceptibility indicates the degree of magnetization in presence of an external magnetic field. The atomic dipoles of a material get aligned when a magnetic field is imposed. In ferromagnetic materials the alignment of atomic diploes are maximized. In un-magnetized state, the atomic dipoles of a ferromagnetic material are randomly organized and the net magnetic field as a whole is zero. If a magnetizing force is applied, the dipoles become aligned. The common properties of ferromagnetic materials are:

1. They have net magnetic moments due to the presence of unpaired electrons.
2. They are easily attracted to magnetic field and retain magnetic properties even after the removal of the field.
3. Large magnetic susceptibility.
4. Typically large magnetic permeability.

Some common examples of ferromagnetic materials are cobalt, nickel, iron, and mu-metal.

2.6.1.1 Effect of Hysteresis Loop and Permeability

A hysteresis loop is often referred to as the B-H curve. This curve shows the relationship between the magnetic flux density B and the magnetic field strength H. The loop is experimentally generated by measuring the magnetic flux density B of a ferromagnetic material while the magnetizing force H is changed. Figure 2-9 shows the typical shape of a hysteresis loop.

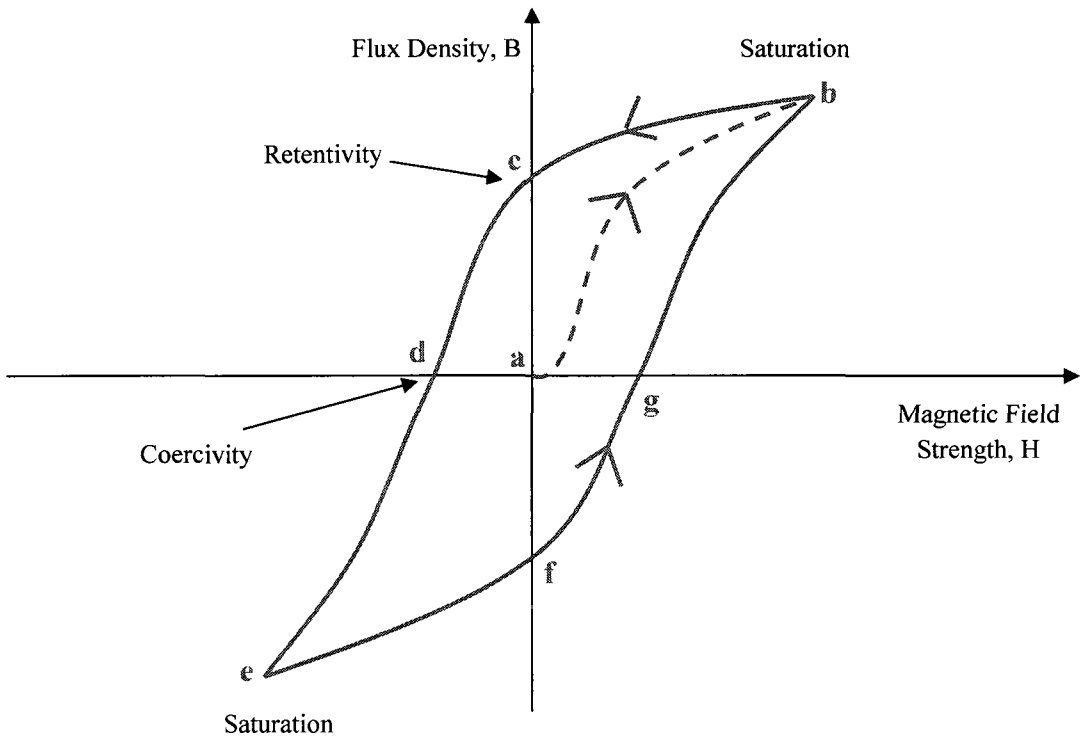

Figure 2-9: A typical B-H curve or Hysteresis loop for a magnetic material

The dashed line 'a-b' in Figure 2-9 indicates that, if a ferromagnetic material is such that it had not been previously magnetized will follow this line as H is increased. Though not linear, it shows that magnetic flux density B increases with the increase in applied field H.

At point 'b' the material has reached the point of magnetic saturation where any additional increase in H will produce very little increase in B. This indicates that all magnetic domains are aligned. The B-H curve will then follow the path 'b-c' when H will gradually be reduced down to zero. When H is zero B still has got some positive value. This phenomenon indicates the level of residual magnetism in the material. This is due to the reason that some domains remain aligned but some have lost the alignment. When H goes +ve to –ve (that is, changes in direction) the B-H curve reaches to point 'd'. Here B is zero though H is a nonzero value. This is called the magnetic coercivity. The magnetizing force has reversed some of the domains so that resultant B is zero. With the increase of H in the opposite direction, the material saturates again at point 'e'. When H changes it direction again the B-H curve follows a different path for the same reasons mentioned already. Finally it reaches point 'b' and forms a loop.

Different magnetic materials show different shapes of B-H curve and are well suited for different applications. For example, materials that have larger loop areas typically have high coercivity values. They are well suited for permanent magnet applications. On the other hand, materials with smaller loop areas have comparatively low coercivity values. They are used for electromagnets, transformer cores, shielding applications.

From the well known relation $B=\mu H$, where μ is the permeability of a material, it is clear that permeability is the slope of the B-H curve and has different values at different points of the curve. For shielding purposes, materials with higher permeability are preferred. Table 2-1 shows range of relative permeability of three common ferromagnetic materials [45].

Ferromagnetic Material	Range of Relative Permeability
Cobalt	70 – 250
Nickel	110 - 600
Iron	150 - 200000

Table 2-1: Range of relative permeability of some common ferromagnetic materials.

2.6.2 Conductive Material

Conductive materials have high electrical conductivity and their relative magnetic permeability is generally very small. They are either diamagnetic or paramagnetic in nature. Diamagnetic materials are those materials that create a localized magnetic field in presence of an externally applied magnetic field. The external magnetic field and the generated magnetic fields are opposite in directions. On the other hand, paramagnetic materials are those materials that are attracted to an external applied magnetic field. Unlike ferromagnetic materials, they can not retain their magnetic property in the absence of an external magnetic field. There are no known materials with both high electrical conductivity and high magnetic permeability at the same time. Table 2-2 shows the conductivity values of some common materials [45].

Name of the Material	Conductivity (Siemens/meter)
Silver	6.3×10^7
Copper	5.9×10^7
Industrial copper	5.8×10^7
Aluminum	3.8×10^7
Industrial aluminum	3.7×10^7
Lead	4.8×10^6
Tin	9.2×10^6
Steel	5.0×10^6-10^7

Table 2-2: Conductivity in Siemens/meter for some common materials

The way conductive materials work as a shielding screen is known as the 'eddy current cancellation technique' as discussed previously. The effect of material thickness and skin depth are discussed next.

2.6.2.1 Skin Depth Effect

Skin depth effect is defined as the phenomenon where alternating currents tend to flow along the surface of a conductor. Skin depth is an inverse function of frequency. For a given frequency, the skin depth is the distance where current density drops to one Neper (Neper is a dimensionless logarithmic unit. For 10 based logarithms unit is dB and for 'e' based logarithms unit is Neper. 1 Neper = 8.69 dB approximately) below than the current density at the surface.

The propagation constant of a plane wave in a conductive material is given by,

$$\gamma = \sqrt{(j\omega\mu_s(\sigma + j\omega\varepsilon_s)} \qquad (2.27)$$

Where σ, μ_s, ε_s are respectively the conductivity, permeability and permittivity of the material. If $\omega\varepsilon_s$ is much smaller compared to σ (which is generally true for conductive material) we have [45],

$$\gamma = \sqrt{(j\omega\mu_s\sigma)} = \frac{1+j}{\delta} \tag{2.28}$$

where,

$$\delta = \sqrt{\frac{2}{\omega\mu_s\sigma}} \tag{2.29}$$

Here δ is the skin depth of the material and is frequency dependent. For a time varying field, field strength decays exponentially inside the material with a decay length of skin depth. Therefore, when the shield thickness Δ is larger than the skin depth δ, high values of shielding effectiveness can be achieved.

2.7 Summary

Upon completing the background review, the key points of magnetic shielding mechanisms, materials used, and properties that are more relevant to this thesis are summarized here:

1. With the advent of new electronic devices and technologies, EMI risks for medical devices have increased and countermeasures are needed.
2. Electromagnetic shielding (often called magnetic shielding due to the dominance of magnetic field in most interfering sources) is an effective countermeasure against EMI sources to ensure accurate operation of some medical devices such as MCG, MEG, and EEG.

3. Magnetic shielding techniques and their performance greatly depend on the potential EMI sources and their frequency. EMI sources with different frequencies require specific techniques.
4. Static shielding is not dependent on source frequency and shielding performance depends on parameters such as relative permeability and material thickness. Increase in permeability and thickness results in more SE.
5. Dynamic shielding is frequency dependent and shielding performance improves with the electrical conductivity of material used. Skin depth of the material should be small compared to the material thickness.
6. At lower frequency, multiple reflection loss term M in equation 2.18 could be negative and can sometimes decrease the level of SE.
7. Incorporate different shielding techniques in a single system could potentially widen its performance in terms of different EMI sources and their oscillating frequency. Use of different materials would be possible in such system and it might solve the problem of lack of materials with both high permeability and conductivity.
8. Development of a technique that might improve the performance of a shielding system can make it possible to use materials with low permeability that are cost effective too.

Chapter 3: Source and Shield Modeling

Mathematical modeling of electromagnetic field sources and magnetic shielding play a significant role in the development of a shielding mechanism. Modeling is the first step towards the design of a shielding system. It also offers an in depth view of the modelled system. The effect of different design parameters on a shielding system can be well understood and predicted by studying the mathematical modeling of the source and the shield itself. This chapter covers the electromagnetic field sources and shield modeling as the first step towards the development of a magnetic shielding mechanism.

3.1 Point Source and Magnetic Dipole Approximation

Many practical applications involve current carrying conductors in loop formation. These loops can be single turn or multi turns. Irrespective of single or multi turn, such current loops can be approximated by a magnetic dipole. The dimension of the current loop is often small compared to the distance of the observation point. In such a case the current loop can be considered as a magnetic point source [54]. Figure 3-1 shows one such arrangement.

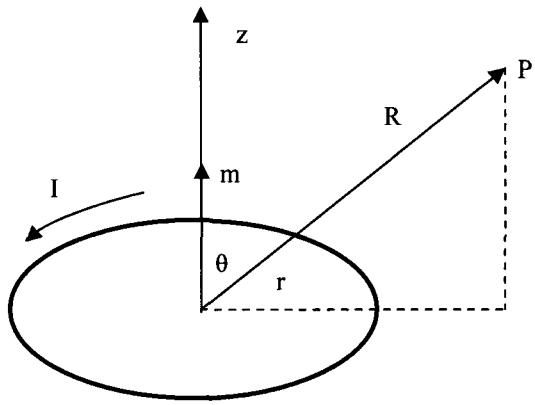

Figure 3-1: Determination of magnetic flux density at point P due to the current I through the single turn current loop

Here, the magnetic moment of the single turn current loop is given by

$$\vec{m} = \vec{a}_z I\pi r^2 \tag{3.1}$$

where, I is the loop current, r is the radius of the loop. Let, $\vec{a}_z$, $\vec{a}_r$ and $\vec{a}_\theta$ are the unit vectors.

Magnetic flux density at point P due to this single loop current coil is given by

$$\vec{B} = \frac{\mu_{air}\vec{m}}{4\pi R^3}(\vec{a}_r\, 2\cos\theta + \vec{a}_\theta \sin\theta) \tag{3.2}$$

The relationship above shows that the magnetic flux density diminishes at a rate of $1/R^3$ from the source. However, their localized magnetic field is comparatively large and can interfere with other equipments activity in the vicinity.

3.2 Biot-Savart's Law and Line Source Modeling

Biot-Savart's law is used to measure the magnetic induction generated by current in steady state condition. Steady state condition means continuous charge flow without any local

charge build up. The law states that the magnitude of differential magnetic flux density $\overrightarrow{dB}$ due to a differential current element I.$\overrightarrow{dl}$ is directly proportional to the vector multiplication of I.$\overrightarrow{dl}$ and unit position vector $\vec{a}_R$. The law further states that flux density is inversely proportional to the square of the distance R between the measurement point P and the current element. The rule of vector multiplication states that direction of dB will be perpendicular to the common plane of $\overrightarrow{dl}$ and $\vec{a}_R$. This means that they form a right handed coordinate system [55]. The law is depicted in Figure 3-2.

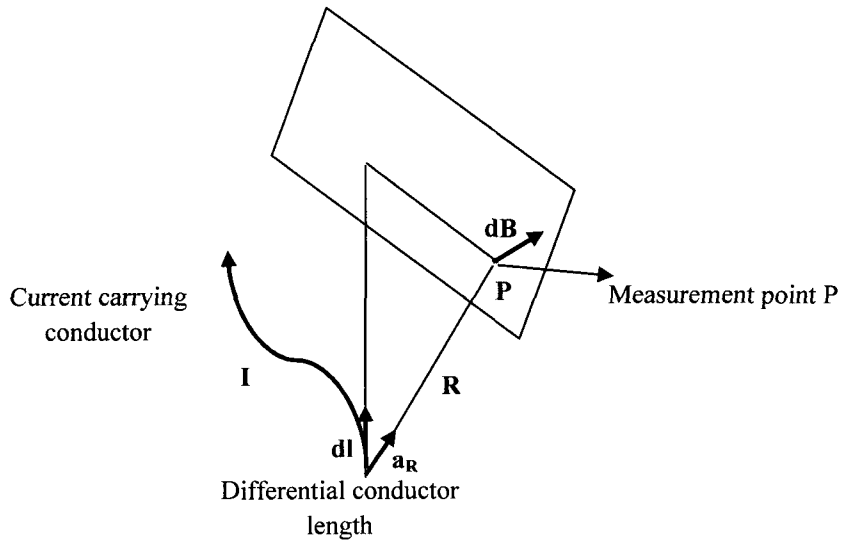

Figure 3-2: Illustration of Biot-Savart's law

Common sources of magnetic field interferences are the current carrying conductors [26;56]. Modeling of magnetic fields generated by current carrying conductors can be simplified if the effect of conductor enclosures and other surrounding structural magnetic materials is neglected [56]. Then conductors can be represented using Biot-Savart's law. According to

Biot-Savart's law, magnetic flux density due to a differential current element $I.\overrightarrow{dl}$ can be written as shown below:

$$\overrightarrow{dB} = \frac{\mu_{air}.I.\overrightarrow{dl}\times\vec{a}_R}{4\pi R^2} \qquad (3.3)$$

where, $\overrightarrow{dB}$ is the differential magnetic flux. The total magnetic flux density $\vec{B}$ can be obtained by integrating the above equation as shown below:

$$\vec{B} = \frac{\mu_{air}}{4\pi} \oint \frac{I.\overrightarrow{dl}\times\vec{a}_R}{R^2} \qquad (3.4)$$

where $\vec{a}_R$ is the unit vector directing from the source to the observation point P, R is the distance, $\vec{B}$ is the magnetic flux density and I is the current.

3.2.1 Single Conductor

Magnetic flux density at a distance R from an infinite length conductor carrying current I can be derived using Ampere's circuital law. Ampere's circuital law relates the induced magnetic field around a current carrying conductor. In integral form, it can be expressed as,

$$\oint B.dl = \mu_{air} I \qquad (3.5)$$

where $\oint$ is the closed line integral in a circular way at distance R. dl is the infinitesimal length and I is the current running through the infinite conductor. By solving the integration we get,

$$B.2\pi R = \mu_{air} I \qquad (3.6)$$

$$B = \frac{\mu_{air} I}{2\pi R} \qquad (3.7)$$

The magnetic flux density for a single conductor is shown in the top left corner of Figure 3-3.

3.2.2 Multiple Conductors

In practice, electric power is generated and distributed for household applications by means of multiple conductor lines. These types of multiple conductors are either in single phase arrangements or in three phase arrangements. The mathematical representations of both single phase and three phase arrangements are given below.

3.2.2.1 Single-Phase Arrangement

A set of two conductors separated by a small distance d and carrying current in opposite directions is known as the single-phase arrangement in electrical circuit. The magnetic flux density B at a distance R for such arrangement can be derived by considering the effect of two conductors separately and getting the overall effect by the law of superposition. Suppose the flux densities produced by two conductors are B_+ and B_- respectively. The overall flux density is given by,

$$B = B_+ + B_- \qquad (3.8)$$

By substituting the value of B_+ and B_- for a single conductor as was shown in equation (3.7),

$$B = \frac{\mu_{air}}{2\pi\,(R - {}^{d}/_{2})} I - \frac{\mu_{air}}{2\pi\,(R + {}^{d}/_{2})} I \qquad (3.9)$$

When R>>d (which is generally true), the above equation can be simplified to,

$$B = \frac{\mu_{air} I d}{2\pi R^2} \tag{3.10}$$

The single-phase arrangement of electrical conductor is shown in the top right corner of Figure 3-3.

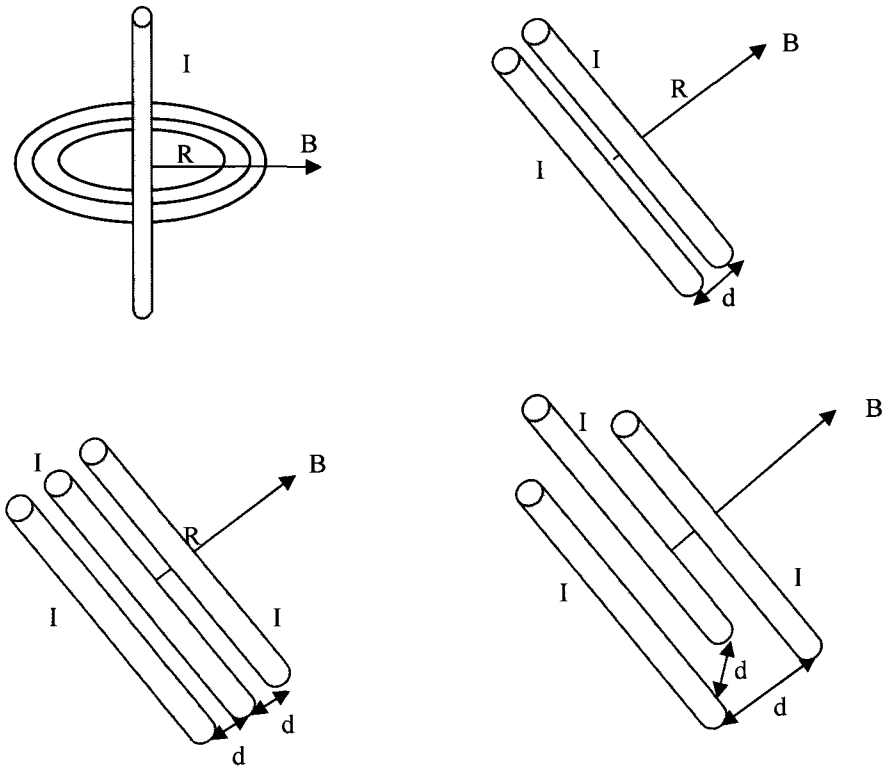

Figure 3-3: Modeling of current carrying line. Top-Left: single conductor. Top-Right: multiple conductors, single-phase. Bottom-Left: Multiple conductors, flat-three-phase configuration. Bottom-Right: Multiple conductors, trefoil-three-phase configuration (adapted from [56]).

3.2.2.2 Three-Phase Arrangement

Often, the electrical power is distributed by means of a three-phase AC transmission system. The arrangement of three conductors can be flat or trefoil. If we consider such three phase system as balanced, voltages and currents of each phase will be 120 degrees apart from each other. For such case, the overall magnetic flux density for flat configuration can be obtained as:

$$B = \frac{\sqrt{3}\mu_{air} Id}{2\pi R^2} \tag{3.11}$$

For trefoil configuration the flux density will be:

$$B = \frac{\sqrt{6}\mu_{air} Id}{4\pi R^2} \tag{3.12}$$

The arrangement of three phase current carrying line is shown in Figure 3-3.

From all the above arrangements (single and three phases) it is evident that the magnetic flux density is directly proportional to the amount of current running through the conductor and their spacing. On the other hand, flux density is inversely proportional to the square of the distance between the source and the observation point.

3.3 Circular Current Loops and Infinite Plate Shield

Here the mathematical modeling and expression for SE of a planar shield in presence of circular current loops is discussed. The arrangement of infinite planar shield and two circular current loops are shown in Figure 3-4. The loop in region 1 is carrying a current I and is known as the source loop or the emitter system. The other loop in region 3 serves as the

detector loop where SE has to be measured before and after placement of the planar shield with thickness Δ, permeability μ and conductivity σ. The expressions will be provided in cylindrical co-ordinates system with unit vector of co-ordinates as i_r, i_φ and i_z . Because of symmetry, magnetic vector potential G has only i_φ component.

The assumptions made here are:

1. Loop radius 'a' is much smaller than the operating wavelength which is particularly true for low frequencies. For example, the coil loop radius used for experiment was 1.65 cm (Chapter 5). The operating wavelengths for 60 Hz and 25 KHz are (4.980×10^8) and (1.196×10^6) cm respectively.
2. The current is approximately uniform along the source loop.
3. The conductivity of the magnetic planar shield is enough that we can neglect the effect of displacement current.

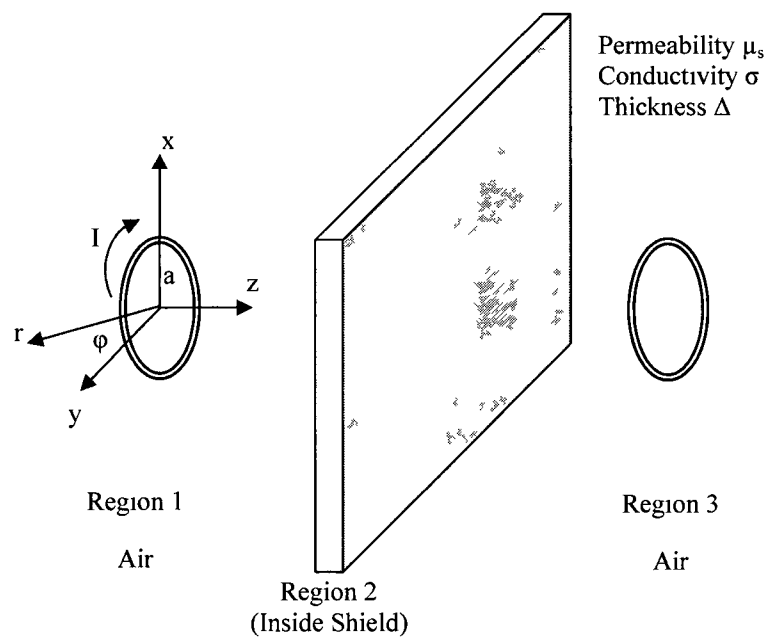

Figure 3-4: Circular current loop perpendicular to an infinite planar shield

Denoting the wave number in air by k_{air} and the propagation constant inside the shielding material by γ, the wave equations can be written as,

$$\nabla^2 G_\varphi + k_{air}^2 G_\varphi = 0 \tag{3.13}$$

$$\nabla^2 G_\varphi - \gamma^2 G_\varphi = 0 \tag{3.14}$$

Where γ is given by $\sqrt{(jw\mu_s \sigma)}$. For cylindrical co-ordinate we have,

$$\nabla^2 G_\varphi = \left(\frac{\partial^2}{\partial r^2} + \frac{1}{r}\frac{\partial}{\partial r} + \frac{\partial^2}{\partial z^2}\right) G_\varphi \tag{3.15}$$

By applying the technique of separation of variables, the general solution of magnetic potential in the three regions (region 1 through 3) can be solved as [45;57;58],

$$G_{\varphi 1} = \frac{\mu_{air} aI}{2} \int_0^{+\infty} \frac{\lambda}{\tau_{air}} J_1(\lambda a) J_1(\lambda r)[e^{-\tau_{air} z} + C_1(\lambda) e^{\tau_{air} z}] d\lambda \tag{3.16}$$

$$G_{\varphi 2} = \frac{\mu_s aI}{2} \int_0^{+\infty} \frac{\lambda}{\tau} J_1(\lambda a) J_1(\lambda r)[C_2(\lambda) e^{-\tau z} + C_3(\lambda) e^{\tau z}] d\lambda \tag{3.17}$$

$$G_{\varphi 3} = \frac{\mu_{air} aI}{2} \int_0^{+\infty} \frac{\lambda}{\tau_{air}} J_1(\lambda a) J_1(\lambda r)\, C_4(\lambda) e^{-\tau_{air} z} d\lambda \tag{3.18}$$

Here, J_1 () is the first order Bessel function, $\tau = \sqrt{(\lambda^2 - \gamma^2)}$, $\tau_{air} = \sqrt{(\lambda^2 - k_{air}^2)}$, C_1-C_4 are functions of λ where λ is an arbitrarily chosen constant. Magnetic flux density at region 3 is

given by, $B = \nabla x G_{\varphi 3}$. By solving B without and with placing the planar shield and using the relationship for SE, one can obtain,

$$SE = 20\ \log_{10}\left[\frac{1}{4\mu_r}\frac{\int_0^\infty \lambda^2 \tau_{air}^{-1} J_1(\lambda a) e^{-\tau_{air} z} d\lambda}{\int_0^\infty C\lambda^2 \tau \tau_{air}^{-2} J_1(\lambda a) e^{-\tau_{air} z-(\tau-\tau_{air})\Delta} d\lambda}\right] \tag{3.19}$$

where,

$$C = \left[\left(\frac{\tau}{\tau_{air}} + \mu_r\right)^2 - \left(\frac{\tau}{\tau_{air}} - \mu_r\right)^2 e^{2\Delta\tau}\right]^{-1} \tag{3.20}$$

The equation (3.19) was solved by Ryan using numerical integration technique [59] and Bannister later showed the equivalence of this equation with equation (2.15) in terms of reflection, absorption and multiple reflection terms [60]. This equation shows the relationship between SE and other parameters such as magnetic permeability, conductivity, current loop radius, and shield thickness. This arrangement was used to run the simulation and experiments. One current loop was energized and served as a magnetic noise source or emitter. The other current loop served as the susceptor or receiver. Considering the equivalence of equation (3.19) and equation (2.15), equation (2.15) is used in explaining the simulation and experimental results for its easy and straight forward relationship with SE. (Equation (2.15) was given by S=R+A+M in chapter 2)

3.4 Summary

The mathematical modeling of common EMI sources and planar shielding in presence of circular current loop sources were covered in this chapter. Here the key points are summarized as:

1. Common sources of EMI can be approximated as point source under the assumption that the dimension of the source is small compared to the distance between source and observation points.
2. Most common sources of EMI are the current carrying conductors and can be modeled using the well known Biot-Savart's law. Such modeling is made by ignoring the effect of conductor enclosures and nearby magnetic materials. This type of modeling offers easy prediction of the source behaviour.
3. SE of a planar shield in the presence of a circular current loop is the function of the material's relative permeability, electrical conductivity, and thickness. Increase in permeability, conductivity, and thickness will result in the increase in SE as shown in the mathematical relationship. SE increases almost linearly with the increase in material thickness.
4. The expression for SE for the simulation and experimental arrangements is given in equation (3.19). This arrangement can be interpreted in terms of reflection, absorption and multiple reflection terms due to the equivalence of equation (3.19) and (2.15).
5. SE is not dependent on the distance between shield and source, which means if the distance between source and observation point is fixed, SE would be equal for placing the shield at any point between the source and observation point.

Chapter 4: Development of the Shielding Mechanism and Simulation Studies

This chapter discusses the workflow diagram towards the development of a shielding mechanism. Simulations that were performed are also covered here along with simulation environments, their impact upon results, and a brief discussion on each simulation trial. Before running the experiments, it is important to design and test experimental setups in a simulation environment. Simulation ensures a more controllable experimental procedure and serves as an initial confirmation of expected results. In previous chapters, mathematical modeling of EMI sources and shielding were covered. This chapter implements these concepts in a simulation environment.

4.1 Systematic Workflow

The development of the proposed shielding system was done in sequential steps. To give a clearer view of the steps involved, the work steps towards the development of the proposed magnetic shielding mechanism are shown in the following flow chart (Figure 4-1):

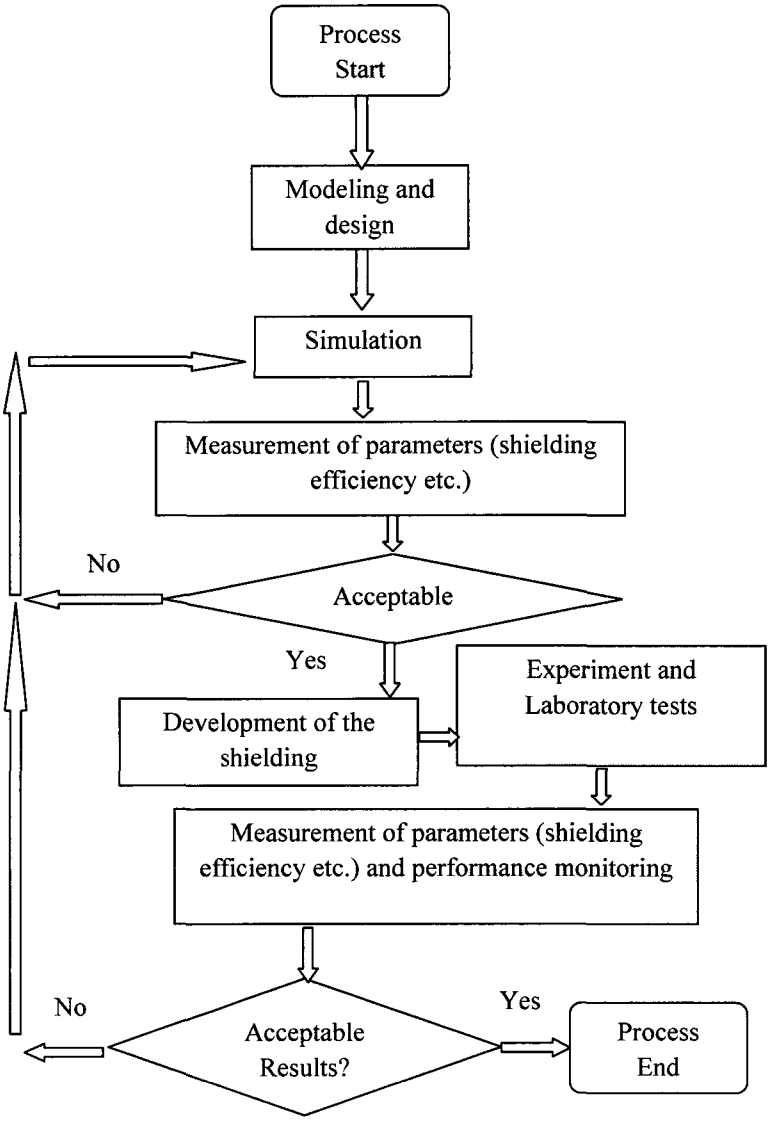

Figure 4-1: Systematic workflow diagram towards the development of a shielding mechanism

4.2 Simulation Studies

All the simulations of this thesis work were done using the electromagnetic simulation tool 'Maxwell 3D v11.1' of Ansoft Corporation (www.ansoft.com). 'Maxwell 3D' is a high-performance interactive software package. To solve three-dimensional (3D) electric,

magnetostatic, eddy current and transient problems, 'Maxwell 3D' uses the Finite Element Method (FEM).

4.2.1 Finite Element Analysis Method

To solve an electromagnetic problem, one has to deal with Maxwell's equations. The field of electromagnetics that deals with the numerical analysis and approximation of Maxwell's equations is known as Computational Electromagnetics. For real world problems, the solution of Maxwell's equations is often complex. Therefore, such problems are generally dealt with using computer aided analysis.

In the thesis work the simulation tool used, adopts the FEM. It is worth mentioning that one has to be familiar with the working principles of the numerical technique adopted so that one can apply the same in an accurate and efficient way. Otherwise application of numerical analysis can even provide inaccurate and inefficient results. Here we will give a brief description of FEM for easy understanding of the design parameters used.

FEM is a numerical method that is applied in different fields to obtain the approximate solution of a given problem. FEM has been used for calculating electromagnetic fields since the 1970's [31]. This method divides the region of interest into smaller two or three dimensional subregions known as the elements. The interconnected elements are known as the mesh. After breaking down the region in finite numbers of elements, the method solves partial differential equations by converting the problem into a system of linear equations. These equations can be cast in the general form:

$$T\,[b] = c \qquad (4.1)$$

where, T denotes the matrix of a set of unknown vectors 'b' and 'c' is the known vector inputs.

These equations are solved for unknown values of 'b' where '*c*' is the known source inputs. In essence, FEM involves the following steps [61;62]:

1. Dividing the region of interest into two or three dimensional finite number of elements (creation of finite element mesh).
2. Forming the general equations of the type shown above for each element.
3. Applying boundary conditions where necessary.
4. Solving the general equation for each element and putting them together.

It is evident from the discussion that by increasing the number of elements we get more accurate results but it increases the computation time and memory needs. For this thesis work, in all simulation solutions, the shielding sample was divided into a minimum of 5000 tetrahedral elements as shown in Figure 4-2.

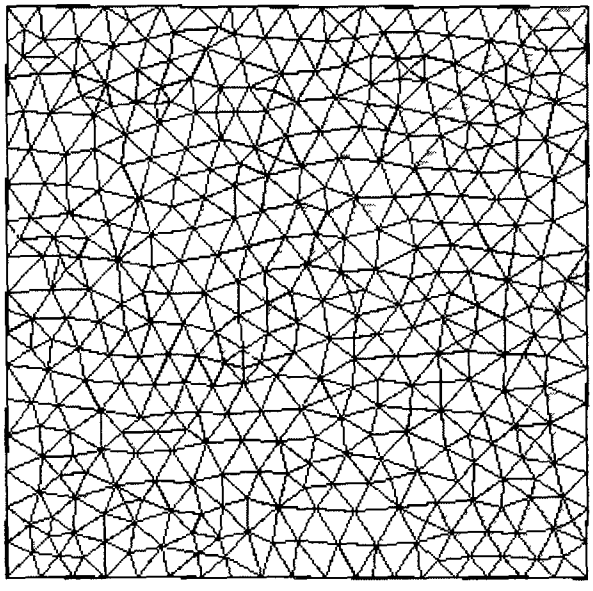

Figure 4-2: Mesh of the region of interest with 0.09 cm thickness (tetrahedral elements)

4.2.2 Design Environment and Parameters

To run the simulations, a region had to be created surrounding all the active design elements. The purpose of this region is to confine the solution from an infinite world to the volume of the region. Also, 'Maxwell 3D' is an adaptive simulation tool where the solution processes is run iteratively before converging to a solution. The 'maximum number of passes' is the maximum number of mesh refinement cycles Maxwell performs. If the maximum number of passes has been completed, the adaptive analysis stops. If the maximum number of passes has not been completed, the adaptive analysis continues unless the convergence criteria are reached. Each pass performs some refinement work in terms of the number of elements if the solution is not within a predefined error limit. Percent error allows one to control the desired solution accuracy. Smaller values produce more accurate but slower solutions. On the other hand, larger values produce less accurate but faster solutions. At each step in the adaptive process, the energy and error energy are computed. After the mesh is refined, the matrix is calculated on the refined mesh. The relative change between the previous matrix and the current matrix is then computed and reported as the matrix delta. The target matrix delta is the percent error. Table 4-1 shows the parameters used in the simulation environment of 'Maxwell 3D'.

Parameter Name	Description
Solution Type	Eddy Current
Maximum Number of Passes	10
Percent Error	1
Percent Refinement Per Pass	15
Minimum Number of Passes	2

Table 4-1: Design environment parameters that were set in the simulation tool 'Maxwell 3D'

For all shielding arrangement designs, frequency was used as the sweep variable with following specifications: Start 1 KHz, Stop 25 KHz, and Step size 2 KHz. In addition, the solutions were also obtained at 60 Hz frequency. Figure 4-3 shows the number of Tets (Tetrahedrons) against the number of pass.

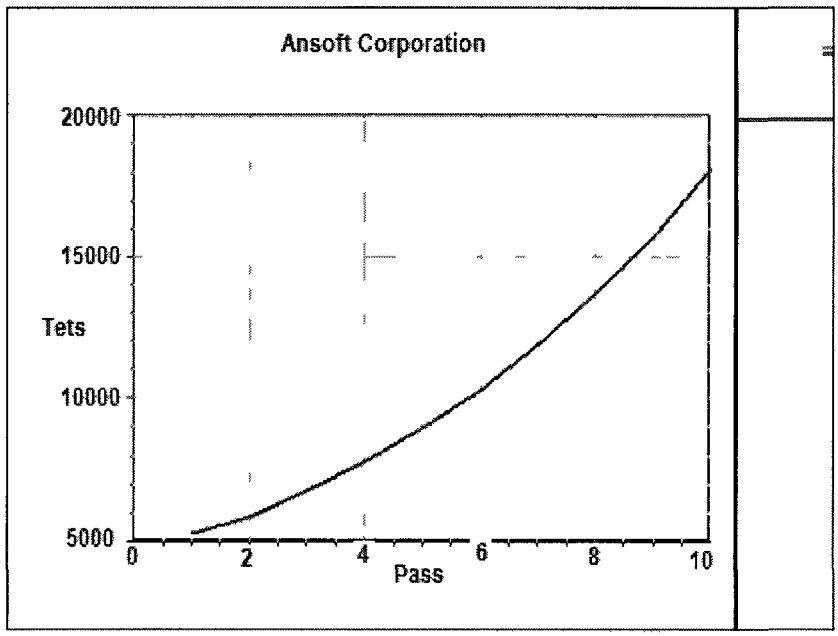

Figure 4-3: Adaptive refinement and increment of number of tetrahedrons per pass

4.2.3 Boundary Conditions

Boundary conditions are fundamental to the solution of Maxwell's equations and also important to understand this solution. The main purpose of assigning boundary conditions are to control the characteristics of planes, faces, or interfaces between objects and forcing the behaviour of an assigned field, to be aware of the assumptions implied by the boundary

conditions and ensure their appropriate enforcement in the simulation. Otherwise the simulation results may be inconsistent.

Ansoft Maxwell 3D solves the field equations that are derived from the differential form of Maxwell's equations. To confirm the validity of the solutions, it is assumed that the field vectors are single-valued, bounded, and have a continuous distribution along with their derivatives. Boundary conditions define the field behaviour across discontinuous boundaries as along boundaries, the fields are discontinuous and the derivatives have no meaning.

In this simulation work, there were two types of boundaries: user defined and automatically defined (defined by the simulation software). Tangential H field was input as the user defined boundary. This boundary was used to assign a predefined magnetic field source H=200 A/m. The solver used in the simulation was the eddy current solver. There were two automatically defined boundaries for this type of solution: Natural boundary and the Neumann boundary.

Natural boundary conditions are applied at the interface between different objects. Ansoft Maxwell 3D automatically enforces these types of boundaries. Where there is a sudden change in the material properties (for example if two or three layers of materials are used), the natural boundary condition reflects the particular local form of Maxwell's equations at the interface between objects. When crossing such a surface of discontinuity, Maxwell assumes the following behaviours:

1. The normal component of magnetic flux density B is continuous.
2. The tangent component of magnetic field intensity H is continuous.
3. The normal component of charge density D has a jump equal to the local superficial charge density.

For magnetic field problems, the Neumann boundary condition specifies that the normal component of the magnetic field intensity H is zero. This necessarily implies that boundary condition confines the magnetic field within the space of the problem [63]. In simulation work, a problem region was defined that surrounds the source, measuring point and the shielding system. The outmost surfaces of the problem region automatically take a Neumann boundary condition to limit the solution region from infinite world to finite design region. Neumann boundaries were assigned to the outside edges of the problem region. Figure 4-4 shows how Neumann and Normal boundary conditions were applied in a design.

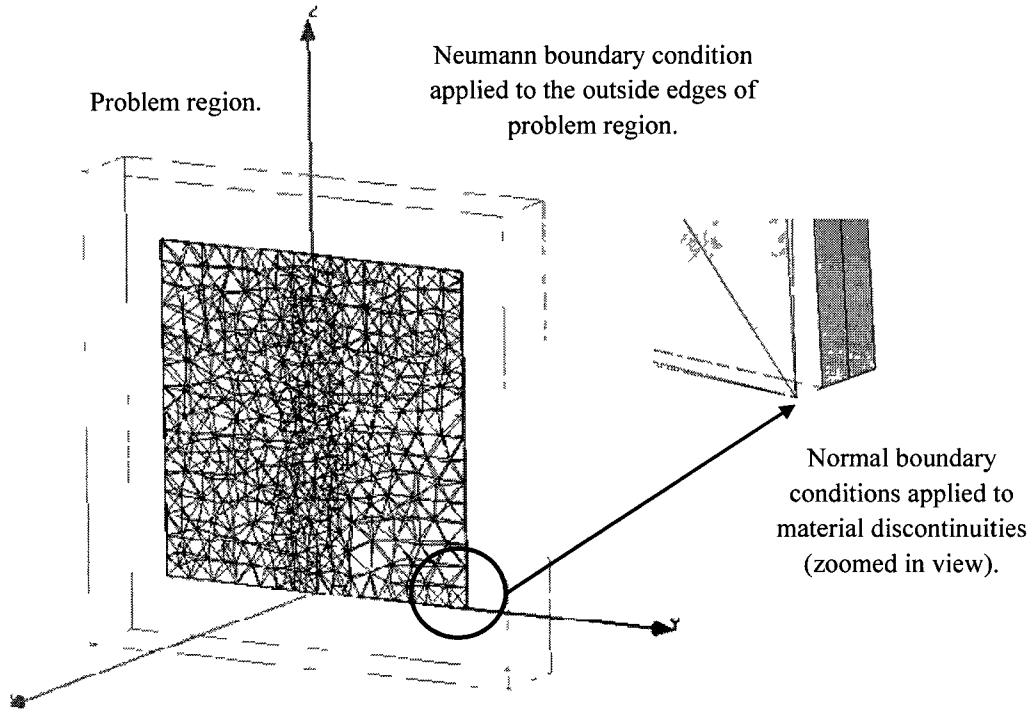

Figure 4-4: Application of Neumann and normal boundary conditions in the design

4.2.4 Parametric Model Creation

The experimental setups that will be performed were mimicked in the simulation tool. The parametric models for the shielding materials were created in the graphics area of the Ansoft 3D modeler. All the shielding samples were modeled as planar sheets of dimension (25 cm x 25 cm x Δ), where 'Δ' is the thickness of the material. Two materials were used: cold rolled steel (CR Steel) as the magnetic material and aluminum (Al) as the conductive material. Thickness Δ for different samples of CR steel was 0.18 cm, 0.09 cm, and 0.06 cm. For aluminum Δ was equal to 0.08 cm. The relative permeability and conductance of CR steel were set to 300 and 9,860,000 siemens/meter respectively. The conductance of Al was set to 20,650,000 siemens/meter.

The source was approximated as a point source and was set such that the emitting magnetic field strength was 200 ampere/meter. The distance of the shielding sample was set to 2 cm from the emitter or the source and measurements were taken at a point 3.5 cm from the source. The ratio of the magnetic field strength without and with placing the shielding in between source and observation point when converted to dB (decibel) gave the value of shielding effectiveness (SE). This is according to the definition of the SE. SE was measured for different frequencies, material dimensions and properties, to investigate the effect of changing different parameters.

4.3 Investigation of Material Type and Property

It has already been discussed and shown mathematically in the previous chapters that different materials have different effects on the total performance and SE profile of the shielding system. As a starting point to the simulation work, the material type and its

properties were investigated to confirm the level of impact they have on SE of a shielding design.

An increase in permeability of a magnetic material was expected to increase SE. The same is true for conductive material where SE increases with the increase in material conductivity. Four parametric models were created. Two with magnetic material CR steel with relative permeability of 400 and 300 respectively. The other two were conductive material Al with conductivity of 33,000,000 siemens/meter and 20,650,000 siemens/meter respectively. For CR steel, shielding plate dimensions were kept constant at (25 cm x 25 cm x 0.18 cm) and for Al at (25 cm x 25 cm x 0.08 cm).

The SE vs frequency curve showed the clear superiority of samples with higher permeability and conductivity (Figure 4-5 and Figure 4-6). If the relative permeability of CR steel was increased with a value of 100, the average value of SE over the shown frequency range increased by 6.5% (Figure 4-5). On the other hand, by increasing the conductivity of Al from 20,650,000 siemens/meter to 33,000,000 siemens/meter, the average value of SE over the shown frequency range increased by 6.54% (Figure 4-6).

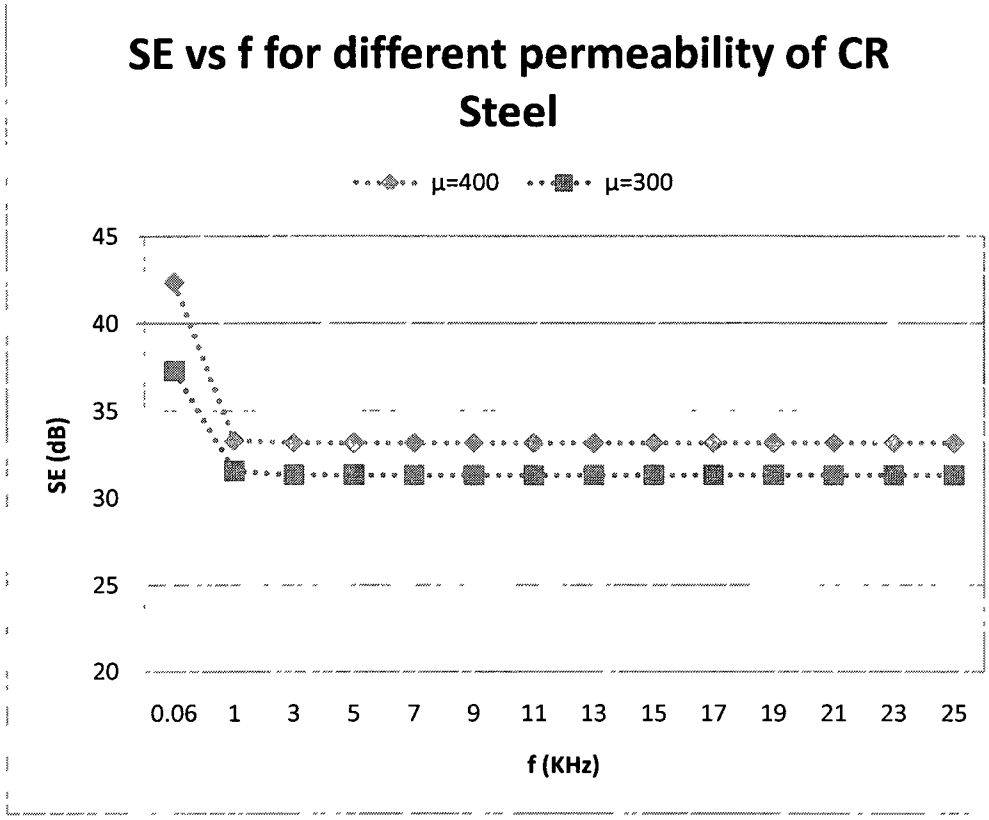

Figure 4-5: Simulation data plot of SE against frequency for different permeability of CR Steel

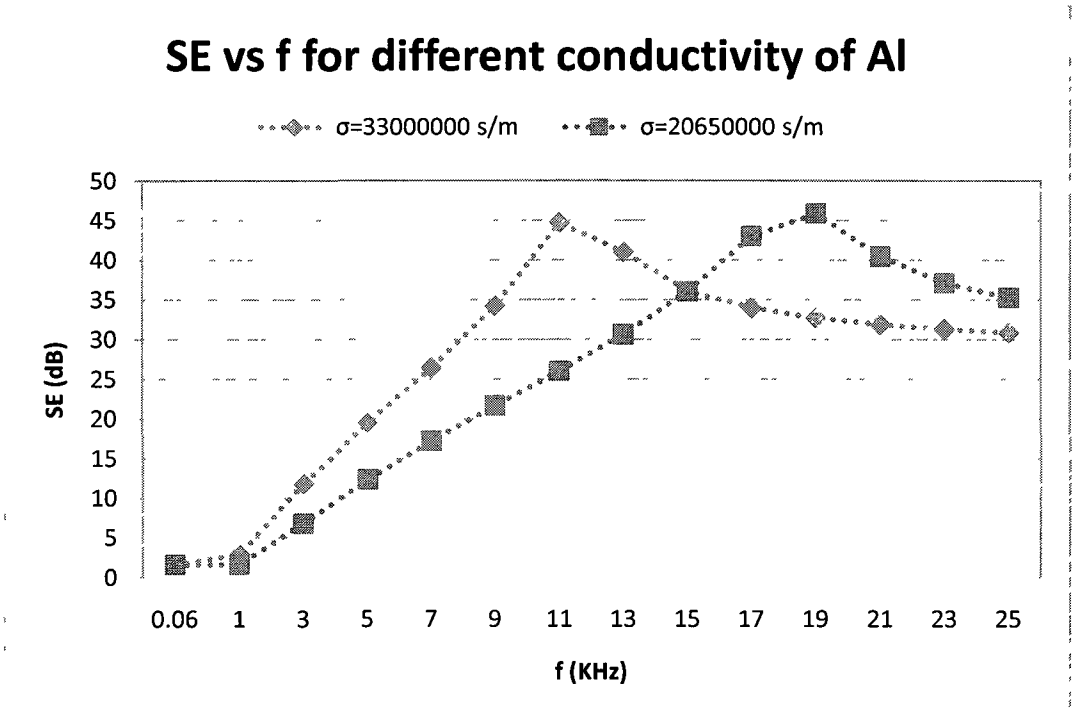

Figure 4-6: Simulation data plot of SE against frequency for different conductivity of Al

4.4 Investigation of Frequency Response

In the next step, the frequency response for SE of CR steel and Al were investigated. It was found that SE profile for CR steel was almost flat except at the lower frequency range. This was interpreted as the combined effect of 'R' (reflection), 'A' (absorption), and 'M' (multiple reflection) terms that was discussed earlier under equation (2.16, 2.17, and 2.18). Though at higher frequency the effect of 'M' is negligible, at lower frequency range 'M' can even add some negative value to the total loss. As a result, SE for CR steel is lower at low frequency, increases as the effect of 'M' is less at higher frequency, and at high frequencies become almost constant. For conductive material Al, SE increases with the increase in frequency. As was mentioned, this type of material is well suited to shield against high

frequency EMI sources. For conductive material, skin depth plays an important role in the level of SE (refer to equation 2.29). Skin depth is a frequency dependent function. At low frequency, the value of skin depth is high and is comparable to the thickness of the shield. As a result, SE is relatively low. As the frequency increases, skin depth becomes negligible compared to the shielding thickness. Therefore, SE increases at higher frequencies. The variations of SE with f are shown in Figure 4-7.

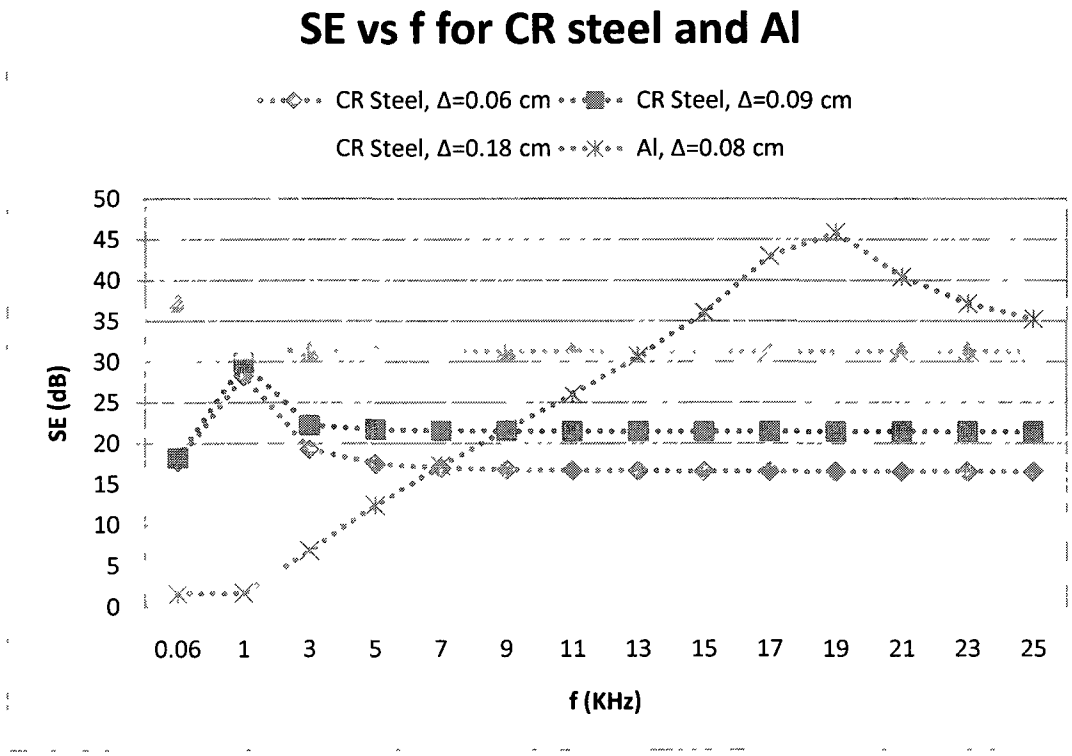

Figure 4-7: Variation of SE with frequency for CR Steel and Al

4.5 Investigation of Material Thickness

To investigate the effect of increasing thickness on SE, simulations were performed on three parametric models of CR steel with thickness values of 0.06 cm, 0.09 cm, and 0.18 cm. It was found that increasing the thickness results in an increase of SE. Generally speaking, SE increases almost linearly with the increase in material thickness. This is due to the absorption loss term A that increases linearly with thickness (equation 2.17, $A = 20\log_{10}(e^{jk_s\Delta})$). In the simulation, the average SE for Δ=0.06, 0.09, and 0.18 cm was found to be 17.77, 21.89, and 31.75 dB respectively. That means that with an increase in Δ by 0.03 cm, SE increased by almost 4.12 dB. Changes in SE for different material thicknesses are shown in Figure 4-8.

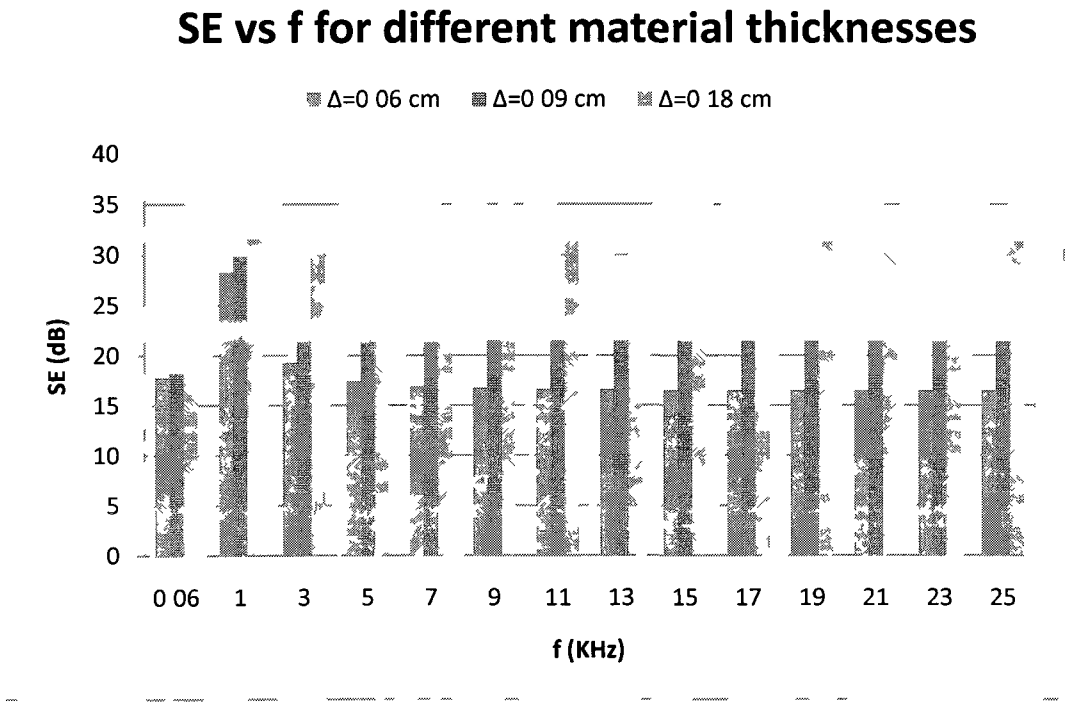

Figure 4-8: Variation of SE with different material thicknesses for CR Steel

4.6 Improvement of SE by Layering

After investigating the effect of different material parameters and frequencies on SE, simulations were run to investigate the effect of layering a shielding system. Here CR steel with thickness, $\Delta = 0.18$ cm was taken as the primary sample. The second sample was a 2-layer shielding system (N=2, N is the number of layer), each layer being 0.09 cm thick. This means that the overall thickness (0.09+0.09) was equal to that of the primary sample. The third shielding sample was a 3-layer system (N=3), each layer being 0.06 cm thick. This means the overall thickness (0.06+0.06+0.06) was again equal to the primary sample. The SE values of different shielding systems at different frequencies are plotted in Figure 4-9.

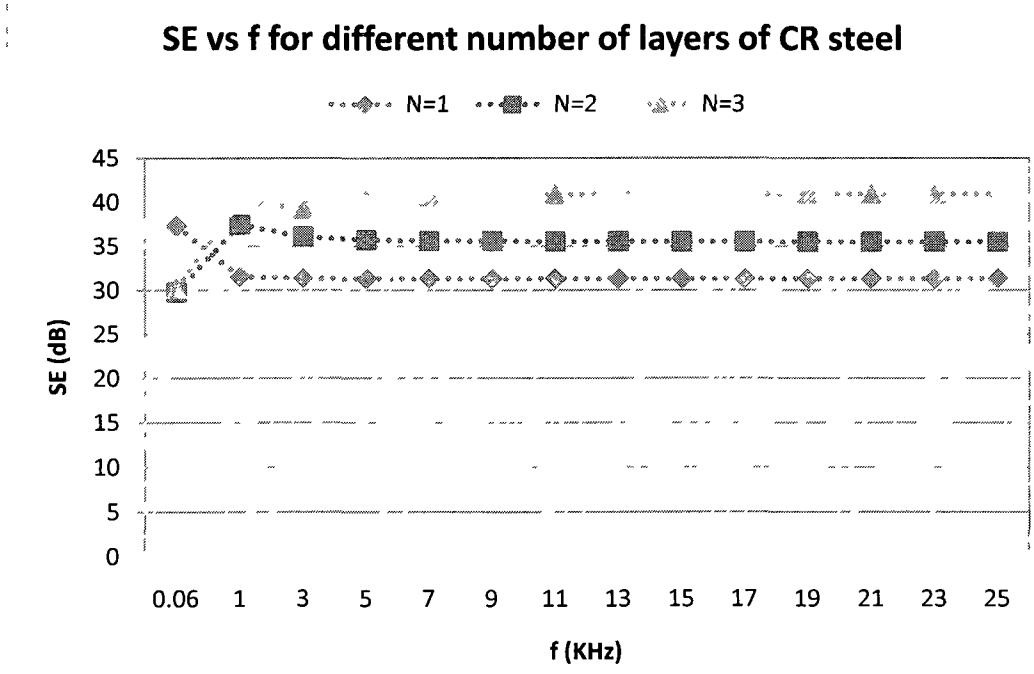

Figure 4-9: Improvement of SE for different number of layering for CR steel

Figure 4-9 clearly indicates that SE can be improved by increasing the number of layers while keeping the total thickness constant. This is due to the reflection loss term R, discussed earlier. Additional layers add more and more reflection loss (refer to equation 2.16). The impinging wave gets attenuated at each air-shield material boundary; therefore the SE of the total system is improved.

Number of Layers	Thickness, Δ	Average SE	% Improvement
N=1	0.18 cm	31.75	--
N=2	(0.09+0.09) cm	35.31	11.21
N=3	(0.06+0.06+0.06) cm	39.88	25.60

Table 4-2: Percent (%) improvement of SE for different number of layers

Table 4-2 shows the percent (%) improvement in average SE for 2 and 3-layer systems over the single layer system. Here percent (%) improvement is calculated by ((final value – initial value) / initial value).

It can be argued that by introducing more and more layers, overall SE can be improved further. While this is true, introduction of each layer will result in additional manufacturing cost and system complexity.

4.7 Investigation of Combined Effect

In the previous step, the simulation results confirmed that the level of SE of a shielding system can be improved considerably by replacing a single layer with two or more layers. This will increase the SE of a given system while keeping the initial thickness the same. Simulations were run to investigate the effect of placing different materials in different

layers while utilizing the SE improvement idea of the previous step at the same time. Three arrangements of shielding samples were used to perform these simulations. All the shielding planar sheets were 25 cm x 25 cm as usual. The ordering is considered from the side of the emitter. The arrangements of the mentioned three configurations were as shown in Table 4-3:

Name	Ordering	Thickness, Δ (cm)
Arrangement#1	CR steel + CR steel + Al	(0.09+0.09+0.08)
Arrangement#2	CR steel + Al + CR steel	(0.09+0.08+0.09)
Arrangement#3	Al + CR steel + CR steel	(0.08+0.09+0.09)

Table 4-3: Three arrangements of shielding to run the simulation in order to investigate the effect of combining different shielding materials and their relative ordering

The average SE of arrangement 1, 2, and 3 were found to be 49.30, 56.67, and 56.02 dB respectively. The SE for arrangement 1 was not as effective in comparison to the other two. This is probably because the inner layer of conductive material Al creates its own localized magnetic field and repulses the EMI source. But the magnetic flux generated by Al will also be cut by the detector coil. This will degrade the shielding performance of the total system to some extent. Between arrangements 2 and 3, it was found that arrangement 2 is particularly better at lower frequency region (up to 9 KHz). As the frequency increases, the shielding performance of arrangement 3 gets better. The conductive material is at the source side and can provide better shielding at higher frequencies. In addition, the magnetic flux created by the Al is attenuated by the internal two layers. The simulation data sets are shown in Figure 4-11.

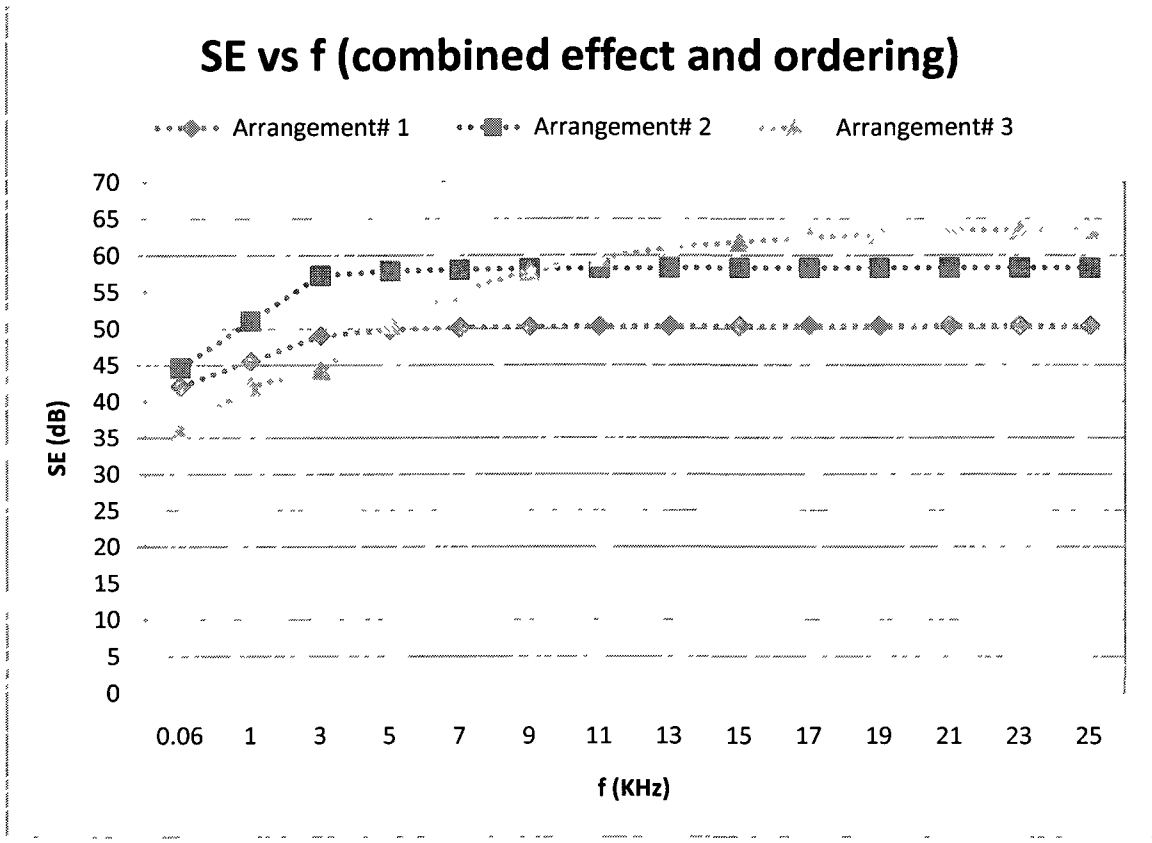

Figure 4-10: Variation of SE with frequency for three arrangements of shielding to investigate the effect of introducing different materials at different layers and their ordering effect

4.8 Summary

The summary and the major findings of the simulation works are:

1. Material properties have a major impact on the shielding performance. Materials with higher permeability and conductivity should be used as long as the material cost does not impose any limitation.

2. SE increases linearly with the increase in material thickness. But improvement of SE by increasing the thickness might not be feasible considering the weight of the material.
3. Addition of conductive material layer improves the frequency response of a shielding system. It makes a shielding system more effective in a wide frequency range.
4. SE can be improved by layering. A two layered shielding system is better in comparison to a single layered shielding system. For 2 and 3 layers, the % improvement of SE was 11.21 and 25.60 respectively. In general, SE improves with an increase in the number of layers. In practice, a shielding system with more layers might not be feasible considering the manufacturing cost and system complexity.
5. A magnetic shielding system with three layers can be realized, in which two layers are made of magnetic materials. By dividing a single layer of magnetic material into two layers, SE can be improved to a certain extent. In addition, conductive material can be utilized in the third layer. Incorporation of a conductive material will improve the SE further and provide better shielding against high frequency magnetic interference sources.

Chapter 5: Experiments

Experiments were performed to validate the findings and results made under simulation works. Experimentations are also important to face the real world conditions. The performance of a shielding system under real world conditions, whether in accordance with the simulation prediction or not can be confirmed by running experiments.

5.1 Experimental Setup

The reference magnetic field noise source was generated by flowing current in a loop of magnet wire. This loop of wire served as the emitter in the system. An ordinary frequency generator was used to excite the emitter with sinusoidal wave of desired frequency. The other magnet wire coil loop was the same as the transmitter/emitter coil loop but served as the detector. This detector was connected to a digital oscilloscope. The loop diameters of both emitter and detector current coils were 3.3 cm. The voltage reading measurements were taken with and without the shielding system in between the transmitter and receiver systems. The relative distances among emitter system, shielding sample and the detector coil were maintained exactly the same as in the simulations. The distance of the shielding sample was

fixed to 2 cm from the emitter current coil or the source and detector current coil was kept at a point 3.5 cm from the source.

The experimental setup for finding the shielding effectiveness of a sample is shown in Figure 5-1.

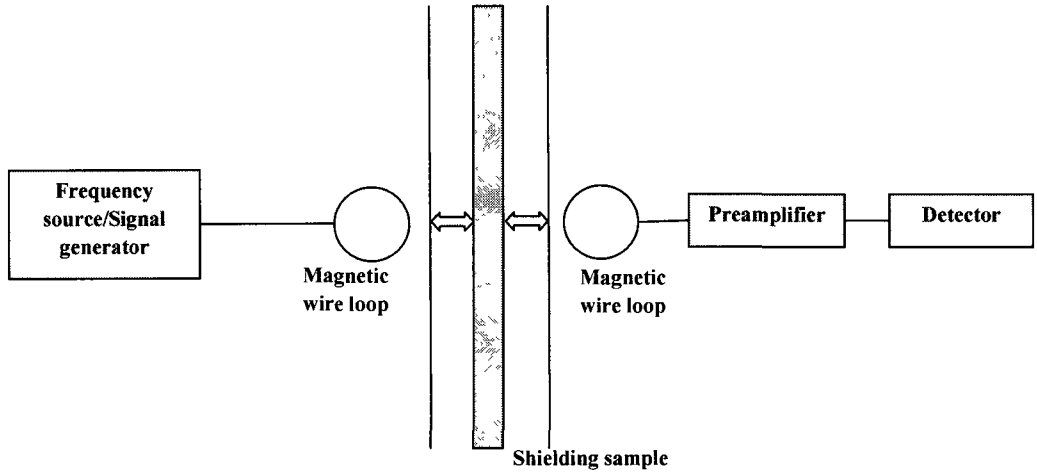

Figure 5-1: Experimental setup for measuring the shielding efficiency

5.2 Equipment and Material Used

The equipments and materials used to run the experiments are shown in Figure 5-2. The individual items are marked with 'A' through 'G' in the figure and a brief description of each item is provided.

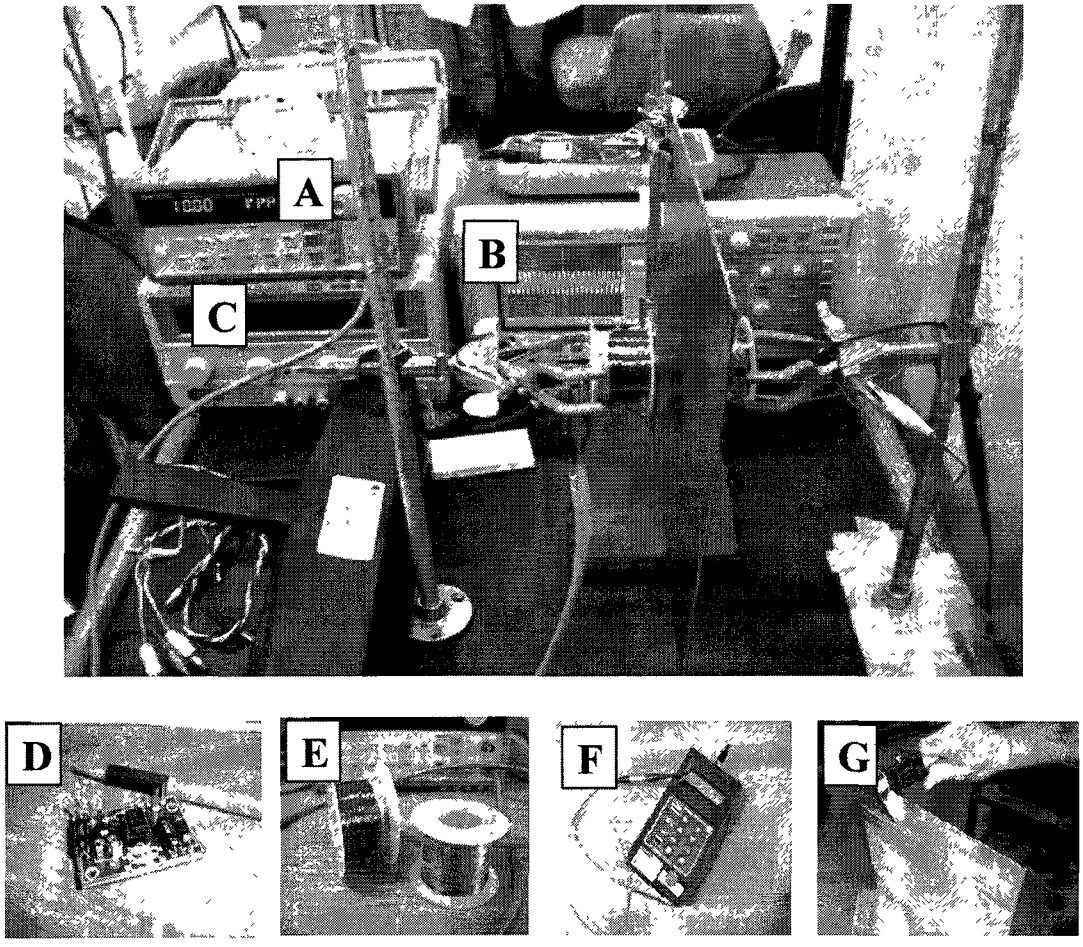

Figure 5-2: Experimental setup and used equipments. A: Function generator. B: Digital oscilloscope. C: DC power supply. D: Preamplifier circuit. E: Emitter and detector current coils. F: Hand-held gauss/tesla meter. G: Digital caliper

A: (Function Generator / Arbitrary Waveform Generator):

HP 33120A function generator was used to energize the emitter coil. It was connected to the emitter coil terminals and supplied the necessary current in the circular loop coil to generate an electromagnetic field source of desired frequency. The waveform used was sinusoidal all

throughout the experiments and the frequency range was varied in between 60 Hz up to 25 KHz. The amplitude of the waveform for each frequency was tuned in a way so that it generates a magnetic field of 200 A/m at the position of detector coil.

B: (Digital Phosphor Oscilloscope):

TDS3000 digital phosphor oscilloscope was used to observe the detected wave shape and measure the signal level for different input amplitude and frequency in the emitter coil. It was connected to the detector coil for some of the setups. In other particular setups, the detector coil was connected to the preamplifier circuit to amplify the signal level and then the output of the preamplifier circuit was connected to the oscilloscope.

C: (Laboratory DC Power Supply):

GPR 1810 HD laboratory DC power supply was used to provide necessary power for the preamplifier circuit for its biasing voltage.

D: (Preamplifier Circuit):

The preamplifier circuit was developed from a standard Velleman kit. The circuit diagram and specifications are provided later under separate heading.

E: (Emitter and Detector Current Coils):

Two spools of magnetic wire were used as the emitter and detector current coils respectively. The emitter coil was standard 28 American Wire Gauge (AWG) magnet wire and the detector coil was standard 31 AWG magnet wire. This specifications are given in Table 5-1.

Parameter Name	Emitter (28 AWG)	Detector (31 AWG)
Conductor Dia (mm)	0.32004	0.22606
Resistance (ohms per km)	212.87	426.73
Max Current Rating (Amp)	1.4	0.7
Max Frequency (KHz)	170	340

Table 5-1: Specifications of the used magnetic wire loops as the emitter and detector

F: (Hand-Held Gauss / Tesla Meter):

F. W. Bell 4048 hand-held gauss / tesla meter was used to confirm the existence of electromagnetic interference near different electronic devices. This was also used to measure the magnetic field strength emitted by the emitter coil at the position of detector coil. This value was used to give input in the simulation tool to mimic the experimental environment.

G: (Digital Caliper):

111-101B standard digital caliper was used to measure the thickness of different shielding materials (http://www.tresnainstrument.com/product/ec16_1606.html). The caliper range was 0-150 mm with 0.01 resolution and 0.03 mm accuracy.

5.2.1 Development of the pre-amplifier circuit

A preamplifier circuit was developed to amplify the signal level detected in the detector coil for some setups. A standard Velleman kit was used to develop the preamplifier circuit (http://www.velleman.eu/distributor/products/view/?id=8897). The amplifier served as a pre-module for a number of experimental setups where the level of signal was insufficient. Figure 5-3 shows the circuit diagram and the preamplifier circuit.

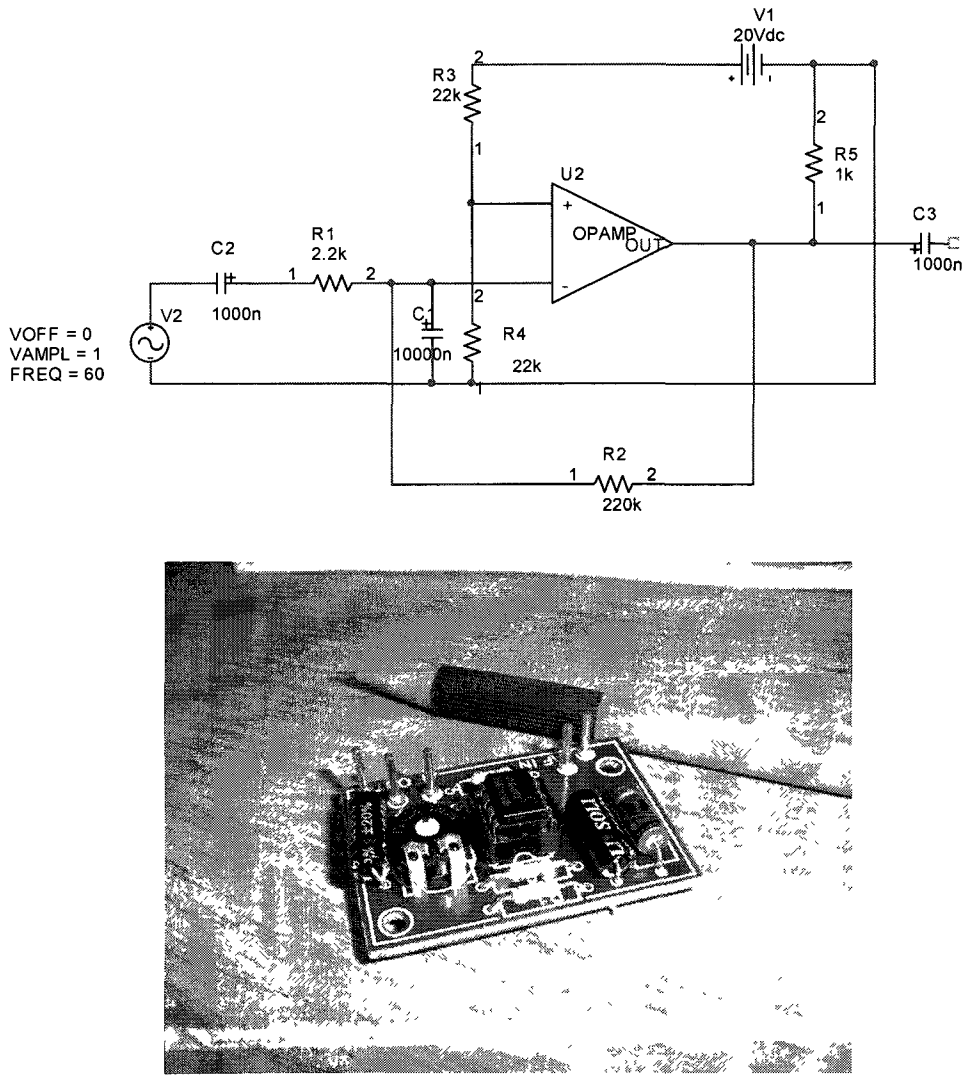

Figure 5-3: Circuit diagram of the preamplifier circuit (top) and the developed preamplifier (bottom)

5.3 Confirmation of EMI problem

Before going through the processes like shielding sample preparation, running the experiment, and data acquisition, existence of EMI was confirmed in various locations using the hand held Gauss / Tesla meter. The Gauss meter mentioned earlier was used for this

purpose. The Gauss meter could confirm the existence of magnetic interferences at various locations and in the vicinity of different electronic devices. Inside the laboratory it could show the existence of magnetic field of 0.4 gauss. This is probably due to the combined effect of earth's static magnetic field and other pieces of electronic equipment emitting magnetic noise. In addition, the detector coil was connected to the oscilloscope without exciting the emitter coil, but it showed voltage noise as shown in Figure 5-4. This is probably due to the superposition of all magnetic noises in the vicinity. These experiments served as a confirmation of the EMI problem.

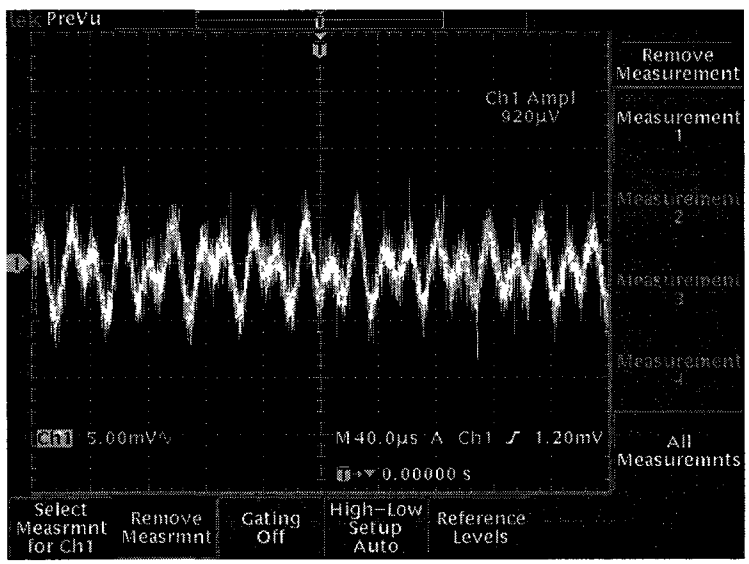

Figure 5-4: Confirmation of EMI. Magnetic noise detected using the detector coil only

5.4 Preparation of the Shielding Sample

The shielding samples were collected and prepared at the facility of 'Russel Metals' (www.russelmetals.com), Ottawa. Some of the samples were collected from 'Metal Supermarkets', Ottawa (www.metalsupermarkets.com). All of the shielding samples were

plane square sheet of 25 cm x 25 cm to be in accordance with the parametric model in the simulations. The following samples were made (Table 5-2):

Material	Grade	Dimension	No. of Samples
CR Steel	A366	(25 x 25 x 0.18) cm	1
CR Steel	A366	(25 x 25 x 0.09) cm	2
CR Steel	A366	(25 x 25 x 0.06) cm	3
Al	5052H32	(25 x 25 x 0.08) cm	1

Table 5-2: Shielding samples prepared for the experiments

Al was chosen due to its low density and cheaper price in comparison to the other most commonly used conductive material copper. A366 grade CR steel was chosen due to its cheap price yet good magnetic property.

5.5 Data Acquisition

In order to obtain the SE value of a sample, the emitter coil was first supplied with sinusoidal signal source of different frequencies. Two voltage readings across the detector current coil were taken for each frequency with and without the placement of magnetic shielding in between the emitter and detector current coils. Let the voltage readings be V_{with} and $V_{without}$ respectively. For a given current and frequency, the generated magnetic field strength H is proportional to the induced voltage V in any current coil and vice-versa. As a result, SE was defined as,

$$SE = 20\log_{10}\left(\frac{V_{without}}{V_{with}}\right) \qquad (5.1)$$

Each experimental SE value represents the mean of three SE values for same frequency and excitation.

5.5.1 Frequency Response

The frequency responses of CR steel of three different thicknesses and Al were found experimentally. Frequency was varied from 1 KHz up to 25 KHz in 2 KHz increments. In addition, the response at 60 Hz was also measured. For CR steel the SE curves were almost flat except for the low frequency but for Al the SE curve gradually increased with frequency. These SE curves trends were in accordance with the simulation results. It was previously argued that SE of CR steel is poor at lower frequency due to the effect of multiple reflection term 'M' which could be negative at lower frequency. The same argument applies here as well. For Al, skin depth is higher at low frequency and vice versa. As a result, SE increases with increasing frequency. The variation of SE with frequency is shown in Figure 5-5.

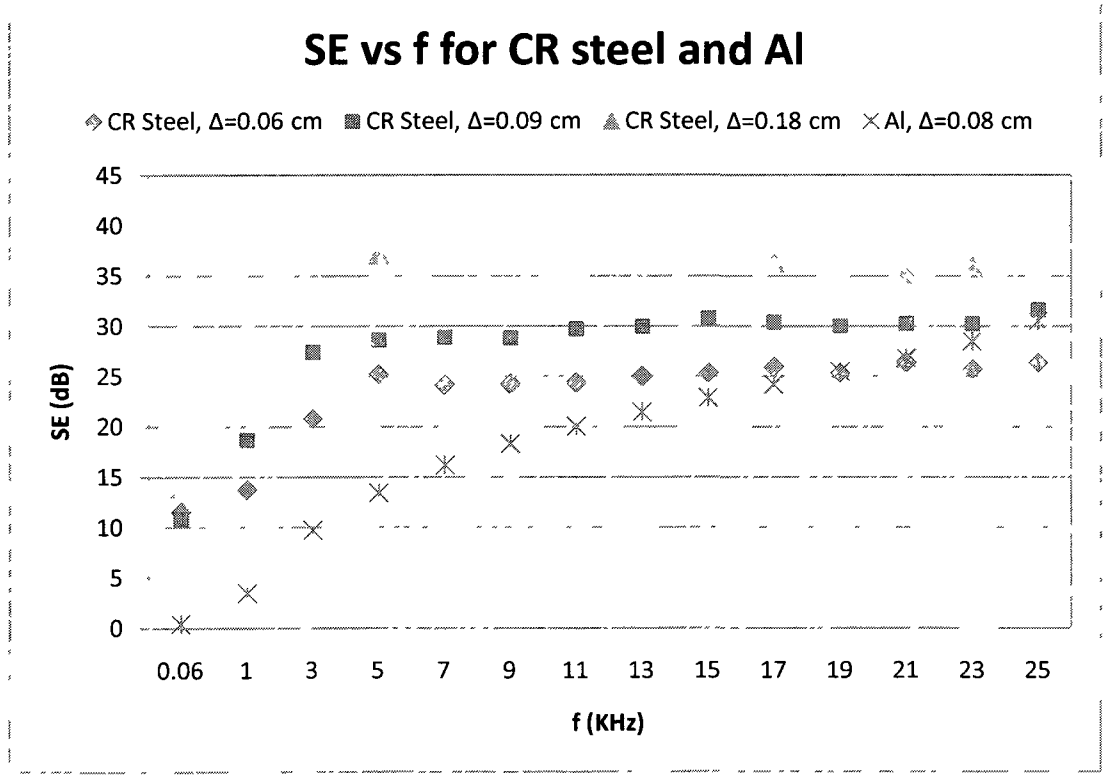

Figure 5-5: Experimentally found SE for CR steel and Al for different frequency

5.5.2 Material Thickness

SE for different thickness of CR steel was calculated. The thicknesses were Δ = 0.06, 0.09, and 0.18 cm. SE increaseed with material thickness as predicted by the mathematical modeling and simulation results. The average SE for Δ=0.06, 0.09, and 0.18 cm was found to be 23.17, 27.59, and 34.68 dB respectively. However the improvement of SE was not entirely linear with the increment in thickness as predicted by the mathematical modeling, equation (2.17) and simulation results. Figure 5-6 shows the variation of SE with material thickness Δ.

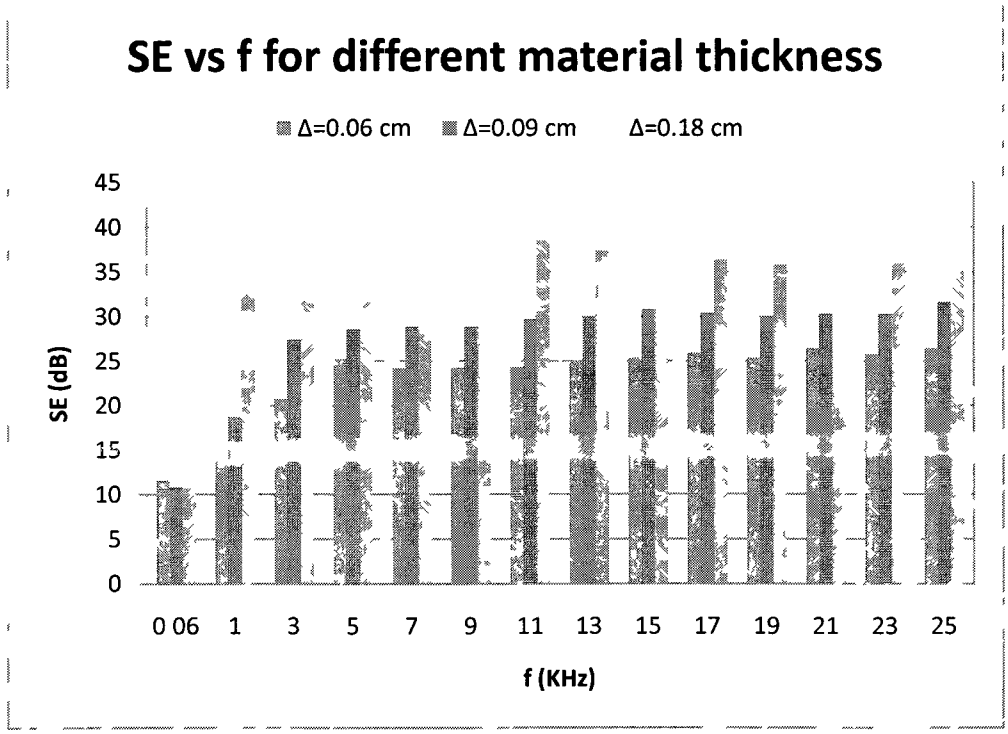

Figure 5-6: Experimentally found SE for CR steel for different material thickness

5.5.3 Improvement of SE by Layering

Three different configurations were prepared to investigate the effects of layering a shielding system. SE was plotted for single, two and three layer system of CR steel where the total thickness was kept fixed at 0.18 cm. The plotted dataset clearly indicated an improvement in SE for two layered and three layered system over the single layer system. Each experimental SE value represents the mean of three SE values for same frequency and excitation. The percent (%) improvement in average SE for 2 and 3-layer systems over the 1-layer system is shown in Table 5-3. Here percent (%) improvement is calculated by ((final value – initial value) / initial value). For a two and three layer system, the percent (%) improvement was 11.2% and 18.57% respectively over a single layer system of equivalent thickness. Figure 5-7 shows the improvement of SE for different number of layering of CR steel.

Number of Layers	Thickness, Δ	Average SE	% Improvement
N=1	0.18 cm	34.68	--
N=2	(0.09+0.09) cm	38.56	11.20
N=3	(0.06+0.06+0.06) cm	41.13	18.57

Table 5-3: Percent (%) improvement of SE for 2 and 3 layer system

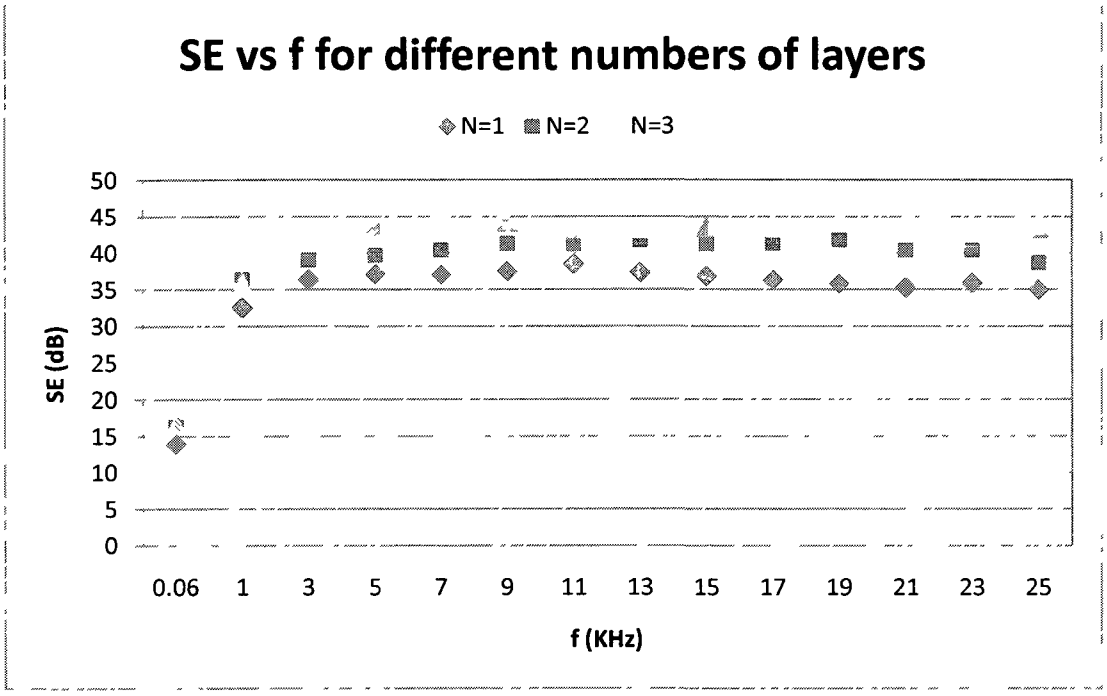

Figure 5-7: Experimental results for SE improvement by layering

5.5.4 Combined Effect

As in the simulation studies, three arrangements of shielding materials were made and experimentally tested as shown in Table 5-4. The ordering is considered from the side of the emitter.

Name	Ordering	Thickness, Δ (cm)
Arrangement#1	CR steel + CR steel + Al	(0.09+0.09+0.08)
Arrangement#2	CR steel + Al + CR steel	(0.09+0.08+0.09)
Arrangement#3	Al + CR steel + CR steel	(0.08+0.09+0.09)

Table 5-4: Investigation on the effect of combining different shielding materials

The average SE of arrangement 1, 2, and 3 were found to be 43.67, 46.29, and 47.38 dB respectively. Arrangement 1, where conductive material Al was kept on the detector side was found less effective in terms of SE. This is due to the reason that, local magnetic field created by the Al was interfering the detector coil. The average SE for arrangement 3, where conductive material Al was kept on the emitter side, was found more effective. The increase of SE with the frequency was more prominent in arrangement 3 than in arrangement 2. The SE for the combined system's three configurations are shown in Figure 5-8.

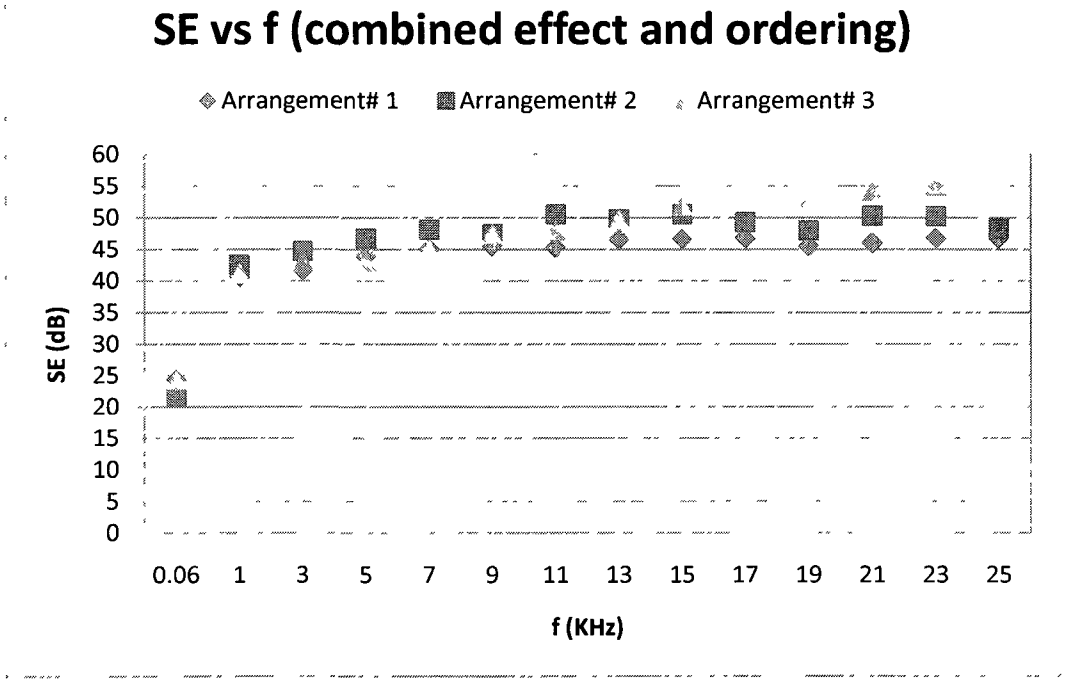

Figure 5-8: Investigation on the effect of combining different shielding materials

5.6 Summary

The findings of the different experimental results are summarized as:

1 SE increased with the increase in material thickness but unlike simulation results the improvement in SE was not entirely linear.

2 Addition of conductive material layer improves the frequency response of a shielding system. It makes a shielding system more effective in a wide frequency range.

3 SE can be improved by layering. A two layered shielding system is better in comparison to a single layered shielding system. For 2 and 3 layers, the percent (%) improvement of SE observed by running the experiment was 11.20 and 18.57 respectively. The improvement for a two layer system was almost following the simulation results but results for a three layer system were less comparable to the simulation results.

4 As suggested in the simulation work, it was also found experimentally that a magnetic shielding system can be realized with three layers where the magnetic material will be utilized in two layers and conductive material will be incorporated in the third layer.

5 In terms of ordering of different layers, arrangement 3 seems better. For arrangement 3, where Al formed the outer most layer, SE increased more prominently with the increase in magnetic noise frequency. Here the outer layer is working as a conductive coating to the whole system and due to the eddy effect improving the SE with the increase in interfering frequency of the source.

Chapter 6: Comparative Studies

This chapter presents the comparison between the simulation results and the experimental results. Though in most of the cases, the simulation results and the experimental results have shown similar trends in plotted curve, there were some mismatches in the results obtained. The probable reasons for these mismatches are discussed next.

6.1 Difference Table

For simplicity, the average SE, averaged in the observed frequency range, is shown side by side in Table 6-1 for both simulation runs and experimentally obtained results. The data contained in Table 6-1 are also plotted graphically in Figure 6-1.

Serial	Sample Name and Description	Average SE in dB (Simulation)	Average SE in dB (Experiment)
1	CR steel, Δ=0.18 cm	31.75	34.68
2	CR steel, Δ=0.09 cm	21.89	27.59
3	CR steel, Δ=0.06 cm	17.77	23.17
4	Al, Δ=0.08 cm	25.42	18.68
5	CR steel, Δ=(0.09+0.09) cm	35.31	38.56
6	CR steel, Δ=(0.06+0.06+0.06) cm	39.88	41.13
7	CR+CR+Al, Δ=(0.09+0.09+0.08) cm	49.30	43.67
8	CR+Al+CR, Δ=(0.09+0.08+0.09) cm	56.67	46.29
9	Al+CR+CR, Δ=(0.08+0.09+0.09) cm	56.02	47.38

Table 6-1: Comparison between the simulation and experimental data

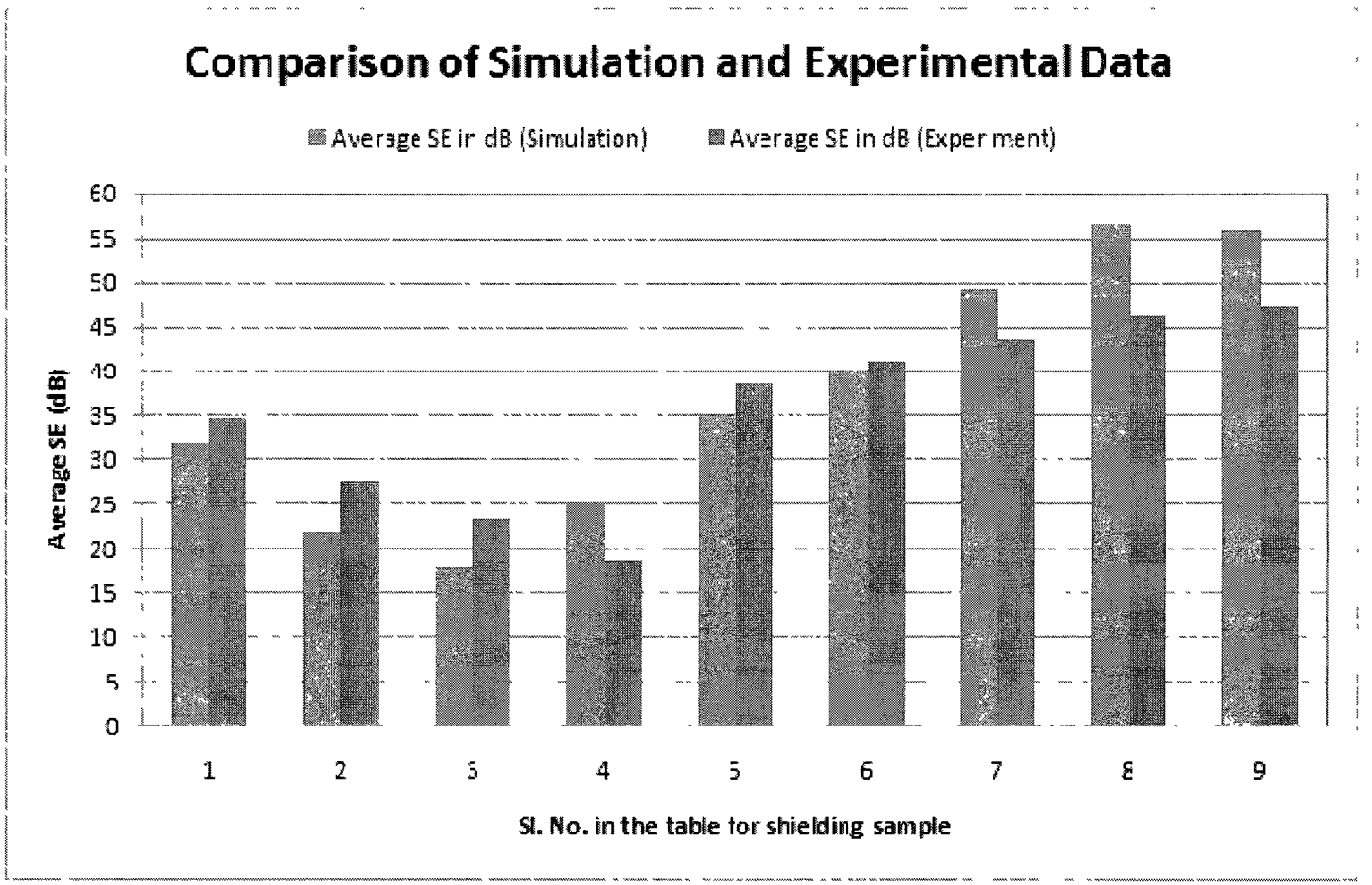

Figure 6-1: Comparison between simulation and experimental data. 1, 2, 3 etc. in the figure refer to the serial number in table 6-1.

6.2 Discussions

The differences in simulation results and experimental results are most likely due to the following reasons:

1 In chapter 3, it was shown mathematically that SE is a function of material properties such as relative permeability, and electrical conductivity. In chapter 4, it was shown by simulation that SE of a shielding system varies with material properties. For example, it was shown for CR steel that with an increase in relative permeability by 100, the average value of SE over the shown frequency range increased by 6.5% approximately. In the simulation studies, the relative permeability was taken as 300. On the other hand, by increasing the conductivity of Al from 20,650,000 siemens/meter to 33,000,000 siemens/meter the average value of SE over the shown frequency range increased by 6.54% approximately. From here it can be argued that the material properties used in simulation was not the same as the original properties of the material used in the experiment. In general, a slight change in material constitution might result in considerable variation in its properties.

2 In simulation studies, a problem region was created where Neumann boundary conditions were applied. The purpose of this region is to limit the solution region from an infinite world to a confined volume. This possibly minimized the amount of magnetic flux leaking over the edges of the sample. But in the experimental setup, it was not possible to limit the amount of flux leakage around the edges of the shielding sample. This might result in the difference in simulation and experimental results obtained.

3 In the simulation environment, the emitter current coil was modeled as a point source. It was done to avoid calculation complexity of the simulation tool and to avoid memory allocation problem. In the experimental arrangement, it was also assumed that the dimension of the circular current coil is small enough to be considered as a point source in comparison to the shielding material's dimension. This assumption might not be entirely true and may contribute to the difference in simulation and experimental results.

6.3 Possible Applications

A three layer magnetic shielding mechanism has been proposed and its performance was investigated by running simulations and experiments. The shielding technique incorporated two different types of materials: CR steel (magnetic material) and Al (conductive material) where two inner layers were made of CR steel and the outer layer of Al (Arrangement#3). The proposed magnetic shielding mechanism improves the SE. Placement of Al at the outer layer has two advantages: (1) due to eddy effect it repulse the interfering magnetic noise source and SE trends to improve with the frequency, (2) the localized magnetic field created by the Al due to eddy effect is reduced considerably by inner two layers of magnetic material CR steel.

The proposed shielding technique can potentially be applied to design and build a compact magnetic shielding. The compact magnetic shielding, enclosing small space, will reduce the level of external magnetic noise interference with the biosignal sensors and increase the signal to noise ratio of the detected biosignal. The compact magnetic shielding has the potential of replacing conventional magnetic shielding room. Since the size, weight and associated cost for a magnetic shielding room is typically high [18] the proposed system has

the potential for overcoming those limitations. One important consideration related to designing a compact magnetic shielding system is its shape. The shielding performance such as shielding effectiveness, magnetic flux leakage, uniformity of magnetic field inside the shielding, manufacturing process, and demagnetization of the shielding depend on the shape of the magnetic shielding [17]. An ideal shape for magnetic shielding is a sphere. But for a spherical shaped magnetic shielding, demagnetizing process and manufacturing is difficult. On the other hand, though cubic shaped magnetic shielding is easy to manufacture, the magnetic field uniformity inside the shielding is not good enough [17;64]. Considering the limitations discussed, a cylindrical shaped magnetic shielding seems preferable.

Possible designs for two compact, cylindrical magnetic shielding, utilizing the shielding technique proposed in this thesis, is shown in Figure 6-2. In addition, the shielding has current coils for applying shaking field. The shaking field would be applied in the middle layer. It would reduce the amount of flux leakage, as the innermost layer would reduce the leakage flux created by the shaking current. The shielding has one end open. This type of shielding design can potentially be used to assist in biosignal measurement where a patient can be slid inside the cylinder through the open end (Figure 6-2a). The provisions for necessary cable connection between the biosignal sensors and other recording device can be made through the open end.

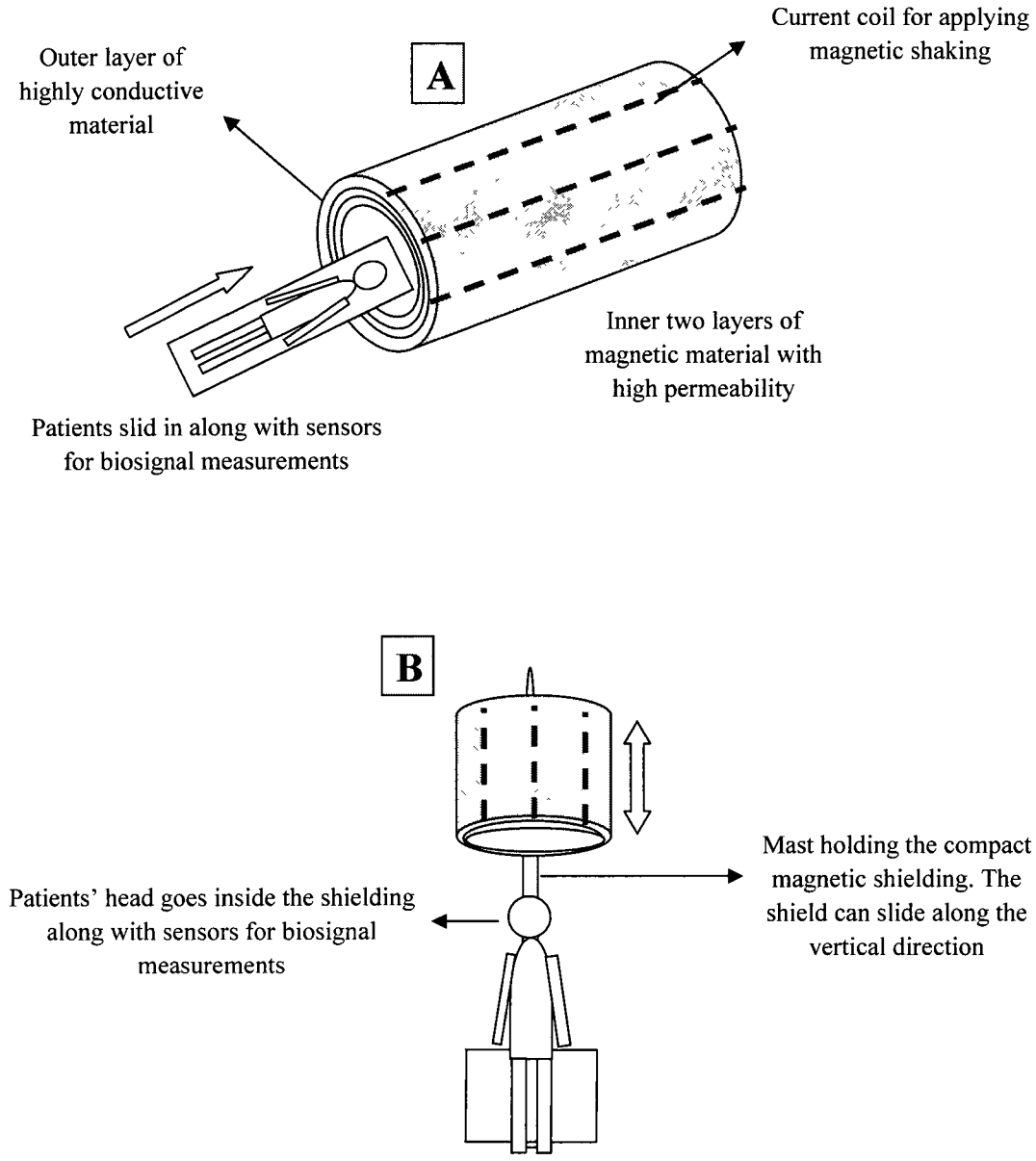

Figure 6-2: Two possible applications of the proposed magnetic shielding mechanism. (A) A compact, cylindrical magnetic shielding where a patient is slid inside the shielding along with array of sensors. This type of arrangement can be well suited for magnetocardiography applications. (B) Compact magnetic shielding in the form of a helmet. This type of arrangement can be well suited for brain signal measurements.

Chapter 7: Conclusions and Future Direction

7.1 Important Findings

Upon completing the simulation studies and experiments, the major findings are given as,

1. It was found that SE of a magnetic shielding system could be improved considerably by introducing a multilayered system. In a multilayered magnetic shielding system, introduction of additional layers increases the surface reflection loss. For a two-layer system the level in SE could be improved by 11.2% compared to a single layer system of equivalent thickness. This was confirmed by the both simulation and experimental results.
2. To improve the frequency response of the system, Al was introduced as a separate layer with the two layer system of CR steel. It makes the shielding system versatile as both magnetic and conductive materials are present in the system. Magnetic material provides shielding against both static and dynamic field sources. On the other hand, conductive material provides shielding against dynamic field sources. It will provide better shielding as the frequency increases. It was observed in both

simulation and experimental results that SE improves with the increase in source frequency.

3. For the ordering of magnetic and conductive materials, arrangement#1 (where conductive material Al layer was on the observation side and other two layers of CR steel were on the emitter side) seems less effective in comparison to the other two arrangements. Arrangement#3, where the conductive layer Al was on the source side and the other two layers of CR steel were on the detector side, yielded more promising results. This is due to the possibility that the conductive layer is pre-screening the impinging wave and any magnetic flux generated due to eddy effect was attenuated by the inner two magnetic layers.

7.2 Future Recommendation

In addition to the research work presented in this thesis, the following recommendations are made:

1 Improvement of SE by a three-layer system can be implemented to develop a magnetic shielding enclosure that would help in accurate operation of medical diagnostic tools such as MEG, and EEG.

2 To develop such a system, a material with higher relative permeability, for example, electrical steel or Mu-metal can be used. It would improve the SE further.

3 Typically, materials with higher relative permeability are costlier too. A study can be performed that deals with the cost analysis for a targeted improvement in SE.

4 The effect of different shapes on the performance of a shielding system can be investigated.

References

[1] Fumal, A. and Schoenen, J., "Current migraine management-patient acceptability and future approaches," *Neuropsychiatric disease and treatment*, Vol. 4, No. 6, 2008, pp. 1043-1057.

[2] Leonardi, M., Steiner, T. J., Scher, A. T., and Lipton, R. B., "The global burden of migraine: measuring disability in headache disorders with WHO's Classification of Functioning, Disability and Health (ICF)," *The journal of Headache and Pain*, Vol. 6, No. 6, 2005, pp. 429-440.

[3] Cook, C. M., Saucier, D. M., Thomas, A. W., and Prato, F. S., "Exposure to ELF magnetic and ELF-modulated radiofrequency fields: The time course of physiological and cognitive effects observed in recent studies (2001-2005)," *Bioelectromagnetics*, Vol. 27, No. 8, 2006, pp. 613-627.

[4] Thiel, F., "Demagnetization of Layered Ferromagnetic Structures for Magnetically Shielding: Frequency Considerations," *IEEE Transactions on Magnetics*, Vol. 45, 2009, pp. 5307-5314.

[5] Wikswo, J. P., "SQUID magnetometers for biomagnetism and nondestructive testing: important questions and initial answers," *IEEE Transactions on Applied Superconductivity*, Vol. 5, No. 2, 1995, pp. 74-120.

[6] Platzek, D., Nowak, H., Giessler, F., Rother, J., and Eiselt, M., "Active shielding to reduce low frequency disturbances in direct current near biomagnetic measurements," *Review of Scientific Instruments*, Vol. 70, 1999, pp. 2465.

[7] Singh, K. D., Holliday, I. E., Furlong, P. L., and Harding, G. F. A., "Evaluation of MRI-MEG/EEG co-registration strategies using Monte Carlo simulation," *Electroencephalography and clinical Neurophysiology*, Vol. 102, No. 2, 1997, pp. 81-85.

[8] Liu, A. K., Belliveau, J. W., and Dale, A. M., "Spatiotemporal imaging of human brain activity using functional MRI constrained magnetoencephalography data: Monte Carlo simulations," *Proceedings of the National Academy of Sciences of the United States of America*, Vol. 95, No. 15, 1998, pp. 8945.

[9] Rosen, B. R., Buckner, R. L., and Dale, A. M., "Event-related functional MRI: past, present, and future," *Proceedings of the National Academy of Sciences*, Vol. 95, No. 3, 1998, pp. 773.

[10] Wikswo, J. P., "SQUID magnetometers for biomagnetism and nondestructive testing: important questions and initial answers," *IEEE Transactions on Applied Superconductivity*, Vol. 5, No. 2, 1995, pp. 74-120.

[11] Pizzella, V., Penna, S. D., Gratta, C. D., and Romani, G. L., "SQUID systems for biomagnetic imaging," *Superconductor Science and Technology*, Vol. 14, 2001, pp. R79.

[12] Saito, T., "Shielding Performance of Open-Type Magnetic Shielding Box Structure," *IEEE Transactions on Magnetics*, Vol. 45, No. 10, 2009.

[13] Nakashima, Y., Kimura, T., and Sasada, I., "Magnetic Field Leakage From a 45 degree-Angle Magnetic Shell and a Reduction Method for a High-Performance Magnetic Shield," *IEEE Transactions on Magnetics*, Vol. 42, No. 10, 2006, pp. 3545-3547.

[14] Sergeant, P., Zucca, M., Dupre, L., and Roccato, P. E., "Magnetic shielding of a cylindrical shield in nonlinear hysteretic material," *IEEE Transactions on Magnetics*, Vol. 42, No. 10, 2006, pp. 3189-3191.

[15] Yamazaki, K., Hatsukade, Y., Tanaka, S., and Haga, A., "Shield Duct to Prevent Magnetic Field Leakage Through Openings in Double-Layered Magnetically Shielded Rooms," *IEEE Transactions on Magnetics*, Vol. 44, No. 11 Part 2, 2008, pp. 4187-4190.

[16] Yamazaki, K., Kato, K., and Fujiwara, K., "Effective combination of magnetic and conductive layers of magnetically shielded room," *IEEE Transactions on Magnetics*, Vol. 36, No. 5, 2000, pp. 3649-3651.

[17] Tashiro, K. and Sasada, I., "A low-cost magnetic shield consisting of nonoriented silicon steel," *IEEE Transactions on Magnetics*, Vol. 41, No. 10, 2005, pp. 4081-4083.

[18] Sasada, I. and Nakashima, Y., "A new method of magnetic shielding: Combination of flux repulsion and backing up magnetic pathways," *Journal of Applied Physics*, Vol. 103, 2008, pp. 07E932.

[19] Burt, E. A. and Ekstrom, C. R., "Optimal three-layer cylindrical magnetic shield sets for scientific applications," *Review of Scientific Instruments*, Vol. 73, 2002, pp. 2699-2704.

[20] Tashiro, K., Nagashima, K., Sumida, A., Fukunaga, T., and Sasada, I., "Spontaneous magnetoencephalography alpha rhythm measurement in a cylindrical magnetic shield employing magnetic shaking," *Journal of Applied Physics*, Vol. 93, 2003, pp. 6733-6735.

[21] Nagashima, K., Sasada, I., and Tashiro, K., "Adaptive compensation of magnetic fields inside an open cylindrical magnetic shield," *IEEE Transactions on Magnetics*, Vol. 39, No. 5 Part 2, 2003, pp. 3223-3225.

[22] Zhao, Z., Zhang, M., Cui, X., and Li, L., "Effect of Wire Grid Covering Aperture on the Shielding Performance of Metal Rectangular Enclosure," *IEEE Transactions on Magnetics*, Vol. 45, No. 3, 2009, pp. 1068-1071.

[23] Saito, T., "Features of a wall with open-type magnetic shielding method," *IEEE Transactions on Magnetics*, Vol. 44, No. 11 Part 2, 2008, pp. 4191-4194.

[24] Fujikura, M., Segawa, K., Chikuma, K., Fujisaki, K., Mino, J., Morita, T., Saito, T., Hirano, H., and Shinnoh, T., "Open-type magnetic shield structure and its performance," *IEEE Transactions on Magnetics*, Vol. 44, No. 11 Part 2, 2008, pp. 4179-4182.

[25] Hirano, H., Saito, T., Shinnoh, T., Fujikura, M., and Chikuma, K., "Shielding Effect of Double-Layered Open-Type Magnetic Shield Structure," *IEEE Transactions on Magnetics*, Vol. 45, No. 10, 2009.

[26] Di, X., Moses, A. J., and Anderson, P., "Measured and computed effect of holes on low-frequency magnetic shielding performance of electrical steel sheet," *IEEE Transactions on Magnetics*, Vol. 42, No. 10, 2006, pp. 3527-3529.

[27] Salinas, E., Atalaya, J., Hamnerius, Y., Solano, C. J., Gonzales, D., Contreras, C., Leon, C., Sumari, M. A., Dimitriou, S., and Rezinkina, M., "A new technique for reducing extremely low frequency magnetic field emissions affecting large building structures," *The Environmentalist*, Vol. 27, No. 4, 2007, pp. 571-576.

[28] Rossi, P., Falsaperla, R., Brugaletta, V., Betti, P., and Gaggelli, A., "Occupational Exposure to Static and ELF Magnetic Fields on Railway Engines," 2003, pp. 31.

[29] Minder, C. E. and Pfluger, D. H.. Leukemia, brain tumors, and exposure to extremely low frequency electromagnetic fields in Swiss railway employees. American journal of epidemiology 153[9], 825-835. 2001. Oxford Univ Press.

[30] Buccella, C., Feliziani, M., Maradei, F., and Manzi, G., "Evaluation of the magnetic field levels produced by a railway line," 2004.

[31] Pekar, J., Netzer, M., and Pekar, Y., "Simulations of ELF magnetic shields," *The Environmentalist*, Vol. 27, No. 4, 2007, pp. 593-601.

[32] Crevecoeur, G., Sergeant, P., Dupre, L., and Van de Walle, R., "Optimization of an Octangular Double-Layered Shield Using Multiple Forward Models," *IEEE Transactions on Magnetics*, Vol. 45, No. 3, 2009, pp. 1586-1589.

[33] Cuntala, J.. Simulation of Electromagnetic Shielding in COMSOL Multiphysics Environment.

[34] Rothwell, E. J. and Cloud, M. J., *Electromagnetics*, CRC 2001.

[35] Pinski, S. L. and Trohman, R. G., "Interference in implanted cardiac devices, part I," *Pacing and clinical electrophysiology*, Vol. 25, No. 9, 2002, pp. 1367-1381.

[36] Waki, H., Igarashi, H., and Honma, T., "Analysis of magnetic shielding effect of layered shields based on homogenization," *IEEE Transactions on Magnetics*, Vol. 42, No. 4, 2006, pp. 847.

[37] Dovan, T., Owen, R., PowerNet, G. P. U., and Melbourne, N. S. W., "Power frequency magnetic fields and computer VDU interference phenomena," 1998, pp. 159-160.

[38] Yamazaki, K., Hirosato, S., Kamata, K., Muramatsu, K., Kobayashi, K., and Haga, A., "Open-Type Magnetically Shielded Room Combined With Square Cylinders Made of Magnetic and Conductive Materials for MRIs," *IEEE Transactions on Magnetics*, Vol. 44, No. 11 Part 2, 2008, pp. 4183-4186.

[39] Hirosato, S., Yamazaki, K., Haraguchi, Y., Muramatsu, K., Haga, A., Kamata, K., Kobayashi, K., Matsuura, A., and Sasaki, H., "Design and Construction Method of an Open-Type Magnetically Shielded Room for MRI Composed of Magnetic Square Cylinders," *IEEE Transactions on Magnetics*, Vol. 45, No. 10, 2009, pp. 4636-4639.

[40] Out, S., "IEEE Standard Method for Measuring the Effectiveness of Electromagnetic Shielding Enclosures,".

[41] Bottauscio, O., Chiampi, M., Roccato, P. E., and Zucca, M., "Sensor, High Frequency, and Power Devices-1-100 kHz Magnetic Shielding Efficiency by Metallic Sheets: Modeling and Experiment by a Laboratory Test Bed," *IEEE Transactions on Magnetics*, Vol. 42, No. 10, 2006, pp. 3533-3535.

[42] Hoburg, J. F., "Principles of quasistatic magnetic shielding with cylindrical and spherical shields," *IEEE Transactions on Electromagnetic Compatibility*, Vol. 37, No. 4, 1995, pp. 574-579.

[43] Hasselgren, L. and Luomi, J., "Geometrical aspects of magnetic shielding at extremely low frequencies," *IEEE Transactions on Electromagnetic Compatibility*, Vol. 37, No. 3, 1995, pp. 409-420.

[44] Basu, B. N., *Electromagnetic theory and applications in beam-wave electronics*, World Scientific Pub Co Inc 1996.

[45] Celozzi, S., Araneo, R., and Lovat, G., *Electromagnetic shielding*, Wiley-Interscience 2008.

[46] Schelkunoff, S. A., *Electromagnetic waves*, Princeton, NJ: Van Nostrand 1943, pp. 223-225.

[47] Erne, S. N., Hahlbohm, H. D., Scheer, H., and Trontelj, Z., "The Berlin Magnetically Shielded Room (BMSR) Section B-Performances," Walter de Gruyter, 1981, pp. 79.

[48] Trenkler, Y., McBride, L. E., Inc, T. I., and Attleboro, M. A., "Shielding improvement by multi-layer design," 1990, pp. 1-4.

[49] Sasada, I., Inoue, I., and Harada, K., "Multipole shaking field for magnetic shielding," *IEEE Transactions on Magnetics*, Vol. 28, No. 1, 1992, pp. 57-60.

[50] Kelha, V., Peltonen, R., and Rantala, B., "The effect of shaking on magnetic shields," *IEEE Transactions on Magnetics*, Vol. 16, No. 4, 1980, pp. 575-578.

[51] Tashiro, K., Nagano, M., Kimura, T., and Sasada, I., "The effect of magnetic shaking on nonoriented silicon steel rings," *IEEE Transactions on Magnetics*, Vol. 41, No. 10, 2005, pp. 4078-4080.

[52] Sasada, I., Kubo, S., OÆHandley, R. C., and Harada, K., "Low frequency characteristic of the enhanced incremental permeability by magnetic shaking," *Journal of Applied Physics*, Vol. 67, 1990, pp. 5583-5585.

[53] Rikitake, T., *Magnetic and electromagnetic shielding*, Springer 1987.

[54] Staelin, D. H., Morgenthaler, A. W., and Kong, J. A., *Electromagnetic waves*, Prentice Hall New York 1993.

[55] Paul, C. R., Nasar, S. A., and Whites, K. W., *Introduction to electromagnetic fields*, McGraw-Hill New York 1987.

[56] Burnett, J. and Yaping, P. D., "Mitigation of extremely low frequency magnetic fields from electrical installations in high-rise buildings," *Building and Environment*, Vol. 37, No. 8-9, 2002, pp. 769-775.

[57] Moser, J. R.. Low Frequency Shielding of a Circular Loop Electromagnetic Field Source. 1966. Navy Underwater Sound Lab New London Conn.

[58] Moser, J. R., Instrum, T., and McKinney, T. X., "Low-frequency low-impedance electromagnetic shielding," *IEEE Transactions on Electromagnetic Compatibility*, Vol. 30, No. 3, 1988, pp. 202-210.

[59] Ryan, C. M.. A Computer Expression For Predicting Shielding Effectiveness For The Low Frequency Plane Shield Case. 1967. Navy Underwater Sound Lab New London Conn.

[60] Bannister, P. R., "New theoretical expressions for predicting shielding effectiveness for the plane shield case," *IEEE Transactions on Electromagnetic Compatibility*, 1968, pp. 2-7.

[61] Silvester, P. P. and Ferrari, R. L., *Finite elements for electrical engineers*, 3rd ed., Cambridge Univ Press 1996.

[62] Huebner, K. H. and Thornton, E. A., *The finite element method for engineers*, Newyork: John Wiley and Sons. 1982.

[63] Cheng, A. H. D. and Cheng, D. T., "Heritage and early history of the boundary element method," *Engineering Analysis with Boundary Elements*, Vol. 29, No. 3, 2005, pp. 268-302.

[64] Harakawa, K., Kajiwara, G., Kazami, K., Ogata, H., and Kado, H., "Evaluation of a high-performance magnetically shielded room for biomagnetic measurement," *IEEE Transactions on Magnetics*, Vol. 32, No. 6, 1996, pp. 5256-5260.